Technische Universität München

Lehrstuhl für
Energiesysteme

Numerical simulation of biomass gasification in a fluidized bed reactor

Diploma Thesis

cand. -Ing. Sotirios Kozalan

Supervisors :	Dipl. -Ing. T. Papadopoulos
	Prof. Dr. -Ing. E. Kakaras
	Prof. Dr. -Ing. H. Spliethoff
Issued :	01.03.2011
Given :	31.08.2011

Eidesstattliche Erklärung

Hiermit versichere ich, die vorliegende Arbeit selbständig und ohne Hilfe Dritter angefertigt zu haben. Gedanken und Zitate, die ich aus fremden Quellen direkt oder indirekt übernommen habe, sind als solche kenntlich gemacht. Diese Arbeit hat in gleicher oder ähnlicher Form noch keiner Prüfungsbehörde vorgelegen und wurde bisher nicht veröffentlicht.

Ich erkläre mich damit einverstanden, dass die Arbeit durch den Lehrstuhl für Energiesysteme der Öffentlichkeit zugänglich gemacht werden kann.

_____, _____ _____

Acknowledgments

This work was entirely developed and supported by the Institute of Energy Systems, at the Technical University of Munich, and the National Technical University of Athens.

From this position, I would like to thank Prof. Dr.-Ing., E. Kakaras, for giving me the opportunity to develop this work in Munich, by approving the Erasmus exchange program. I would also like to thank Prof. Dr.-Ing., H. Spliethoff, for accepting and welcoming me at the Technical University of Munich.

I am grateful to As. Prof. Dr.-Ing., S. Karellas, who, through his incessant efforts and leadership, has led me towards efficient energy technologies and sustainable solutions in Mechanical Engineering. He has stood next to his students by supporting and encouraging them all these years. Special thanks to my supervisor Dipl. -Ing., T. Papadopoulos for his help and expert guidance throughout this research. He has been supporting me about everything I needed from the beginning until the birth of this thesis.

Special mention to my family, who believed in me and loved me all these years. I extend my gratitude to all my loving friends, who stood next to me, and endured numerous simulation talks during the last months.

This work would not have been possible without the Erasmus Program Scholarship, given by the National Technical University of Athens, for which I am deeply grateful.

Abstract

A three-dimensional computational model was developed to describe the biomass gasification process inside a steam fluidized bed reactor. The commercial multi-purpose CFD code FLUENT 13.0 was used, taking into account drying, devolatilization, combustion and gasification processes. Three (3) phases were used to model the reactor (sand, solid phase for the fuel, and gas phase). Sand and solid phase were described using the kinetic theory of granular flows. All phases were described using an Eulerian approach to model the exchange of mass, energy and momentum. The chemical model consists of three (3) heterogeneous and two (2) homogeneous reactions. Drying and devolatilization were supposed instantaneous at the biomass feed region. All reaction-rates were determined by Arrhenius equations, the kinetic parameters of which were found in literature. The gasifier was operated and studied at atmospheric condition. Validation was performed, by comparing the model with experimental results, capturing known phenomena like fluidization bed height, temperature distribution and species concentrations. The main contribution of the presented work is the computational model, which was developed for a three-dimensional biomass gasifier, using a commercial CFD code.

Contents

List of Figures

List of Tables

Nomenclature

Latin letters

Symbol	Unit	Meaning
A	$[1/s]$	Pre-exponential factor
a_i	$[\%]$	Volume fraction of species i
C_D	$[-]$	Drag function
C_{fr}	$[-]$	Friction coefficient
C_P	$[kJ/kgK]$	Specific heat of gas
d_i	$[m]$	Diameter of species i
e	$[-]$	Restitution coefficient
E_a	$[J/kgmol]$	Activation Energy
F	$[N]$	Force
g_0	$[-]$	Radial distribution
h_q	$[kJ/kg]$	Specific enthalpy of phase q
H_g	$[kJ/m^3]$	Heating value of gas
I_{2D}	$[-]$	Second invariant of stress tensor
k_{Θ_s}	$[-]$	Diffusion coefficient
K_{ij}	$[-]$	Momentum exchange coefficient between i and j phase
LHV_i	$[kJ/kg]$	Lower heating value of i
$\dot{m}_{ij}$	$[kg/s]$	Mass transfer from i to j phase
M_s	$[kg/s]$	Solid fuel consumption
p	$[N/m^2]$	Pressure
$\overrightarrow{q_q}$	$[J]$	Heat flux
Q_g	$[m^3/s]$	Volume flow of gas
Q_{ij}	$[-]$	Intensity of heat exchange between i and j phases
R_{ij}	$[N]$	Interaction force between i and j phase
S_i	$[kg/s]$	Source term of mass of phase i
S_q	$[kJ/kg]$	Enthalpy source term
U_{mf}	$[m/s]$	Minimum fluidizing velocity
V	$[m^3]$	Volume

Greel letters

Symbol	Unit	Meaning
γ_Θ	$[J]$	Collisional dissipation energy
ΔT	$[K]$	Temperature difference
η_m	[%]	Gasification efficiency
η_{th}	[%]	Thermal efficiency
Θ_i	$[m^2/s^2]$	Granular temperature of phase i
λ	$[-]$	Stoichiometric ratio
λ_i	$[kg/m \cdot s]$	Bulk viscosity of species i
μ_i	$[kg/m \cdot s]$	Shear viscosity of species i
$\mu_{i,col}$	$[kg/m \cdot s]$	Collision viscosity of species i
$\mu_{i,fr}$	$[kg/m \cdot s]$	Friction viscosity of species i
$\mu_{i,kin}$	$[kg/m \cdot s]$	Kinetic viscosity of species i
ν_i	$[m/s]$	Velocity of species i
ρ_i	$[kg/m^3]$	Density of species i
$\overline{\rho}_i$	$[kg/m^3]$	Effective density of species i
$\overline{\overline{\tau}}$	$[N/m^2]$	Stress-strain tensor
τ_s	$[s]$	Particulate relaxation time
ϕ	$[deg]$	Angle of internal friction
ϕ_{ij}	$[J]$	Energy exchange between i and j phase

Constants

Symbol	Number	Unit	Meaning
R	8.3144621(75)	$[J/molK]$	Ideal gas constant

Abbreviations

Abbreviation	Meaning
ar	As received
$BioHPR$	Biomass Heatpipe Reformer
CFD	Computational Fluid Dynamics
CH_4	Methane
C_2H_2	Acetylene
C_2H_4	Ethylene
C_2H_6	Ethane
C_3H_6	Propylene
CHP	Combined Heat and Power
CO	Carbon monoxide
CO_2	Carbon dioxide
DEM	Discrete Element Method
DNS	Direct Numerical Simulation
GHG	Greenhouse gas
H_2O	Water
$HFCs$	Hydrofluorocarbons
HHV	Higher heating value
$KTGF$	Kinetic Theory of Granular Flows
LES	Large Eddy Simulation
maf	Moist and ash-free
NO_x	Nitrogen oxides
N_2O	Nitrous oxide
PAH	Polycyclic Aromatic Hydrocarbons
$PFCs$	Perfluorocarbons
$RANS$	Reynolds-Averaged Navier-Stokes
Re	Reynolds number
REs	Relative Reynolds number
SF_6	Sulphur hexafluoride
SO_2	Sulphur dioxide
SRS	Scale-Resolving Simulation
$STBR$	Steam to biomass ratio
TOE	Tonne of oil equivalent
$wt\%$	Weight %
$3D$	Three dimensional

Chapter 1

Introduction

1.1 Energy Demand

Modern world and structure of society are inextricably related to energy production. So far, after the industrial revolution in the 18th century, the fuels used for this reason are primarily coal and oil. However, burning fossil fuels releases CO_2 into the Earth's atmosphere. We have clearly changed the equilibrium of natural absorption and emission of CO_2 causing the major problem of global warming that concerns the whole energy society. Arctic shrinkage with subsequent sea level rise, higher average temperatures and intensive weather phenomena are some of the consequences observed the past years. Furthermore, the fossil fuels do not exist in infinite amounts. For these reasons, the need to shift this dependence from fossil fuels to sustainable energy sources is imperative.

The United Nations decided to take measures in order to stabilize the greenhouse gas concentrations in the atmosphere and signed the Kyoto Protocol, on 11 December 1997 in Japan. Under the Protocol, 37 industrialized countries were committed to reduce greenhouse gas (GHG) emissions to an average of 5% against 1990 levels over the five-year period 2008-2012. The Protocol was in force since February 2005. The reduction of carbon dioxide (CO_2), methane (CH_4), nitrous oxide (N_2O), sulphur hexafluoride (SF_6), hydrofluorocarbons ($HFCs$) and perfluorocarbons ($PFCs$) was agreed.

Except for the restrictions placed by the Kyoto Protocol, the recent price rise of crude oil [1] Fig. 1.1 ,(Oil-Price), and scarcity of fossil fuels have led towards the use of alternative energy sources like solar, wind, hydro power, geothermal, and biomass.

Exploitation of biomass for energy production through gasification procedures is an environmentally benign solution. With gasification in general, low-value or waste feedstocks such as biomass, municipal waste, refinery residues, petroleum coke, and generally any carbonaceous compounds can be used to produce heat or power with high efficiency. Specifically, biomass gasification is CO_2 neutral. This is because the carbon content of biomass has been absorbed by the CO_2 of the atmosphere. So the net CO_2 production is zero. The product of gasification is called syngas or product gas. This gas has a high percentage of hydrogen which is advantageous

[1] Brent Crude is the biggest of the many major classifications of crude oil. It is used to price two thirds of the world's internationally traded crude oil supplies. The other well-known classifications (also called references or benchmarks) are the OPEC Reference Basket, Dubai Crude and West Texas Intermediate .

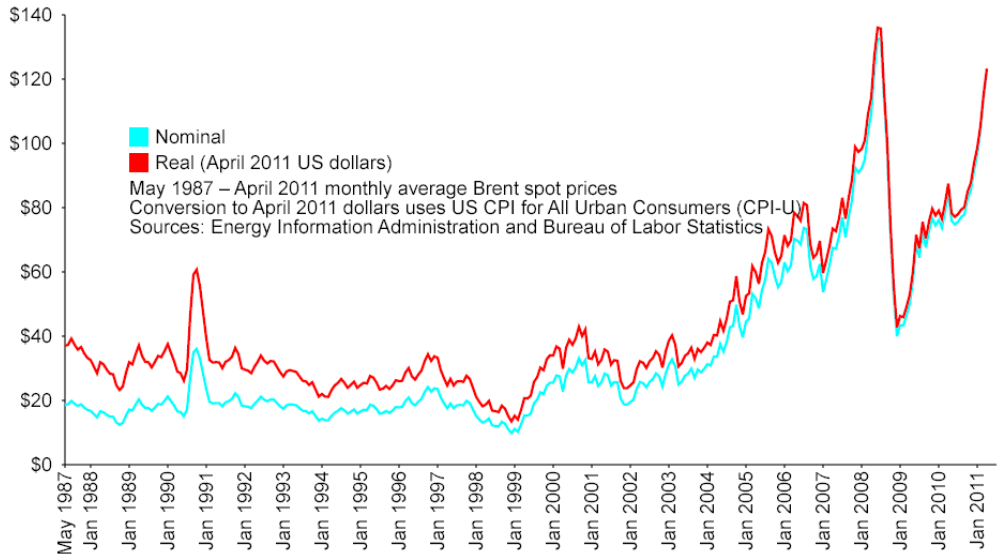

Figure 1.1: Monthly average Brent spot prices from May 1987 - April 2011

to all other fuels because water is the only combustion product. These reasons make biomass gasification a promising alternative for heat and power production.

In Greece, the agricultural and forestry residues are energetically equivalent to 3-4 million tonnes of oil (TOE) annually. The potential of energy crops is of the same or even greater amount. This percentage corresponds to 30-40% of the total annual oil consumption, supposing that 1 ton of biomass has the same heating value as 0.4 tons of oil. However, only 3% of the energy is currently produced from biomass ,Biomass-Potential.

The major advantages from biomass exploitation are :

1. Reduction of CO_2 production. In contrast to fossil fuels, biomass has already engaged it's carbon percentage from the atmosphere through photosynthesis. The CO_2 released, follows a closed loop with no net CO_2 production.
2. Reduction of SO_2, which is released by conventional fossil fuel plants and contributes to acid rain. Biomass has negligible amounts of sulphur.
3. Smaller dependence from external suppliers and enhancement of the energy mixture.
4. Decentralized energy production and job opportunities from the energy crops.

Here, it is worth mentioning that energy crops should not grow against agricultural areas. It is undesired that areas for staple food production are reduced due to fuel production.

The disadvantages of biomass have to do with it's nature :

1. Low energy density because of the high moisture content.
2. Difficulty in collecting, transport and storage compared to fossil fuels.
3. Bigger facilities with more expensive equipment due to low energy density.
4. Seasonal behaviour and quality variation.

These disadvantages along with the obvious CO_2 release for transport and handling of biomass lead to the conclusion that biomass should be utilized close to the sources rather than in central power plants.

Biomass can be exploited in several ways. Each biomass resource has different characteristics in terms of calorific value, moisture and ash content, that requires appropriate conversion technologies for bioenergy production. These conversion routes use chemical, thermal and/or biological processes. Finally, biomass can be classified according to its end use as follows (Bioenergy-routes). The work presented here follows the gasification of solid biomass for fuel gas production.

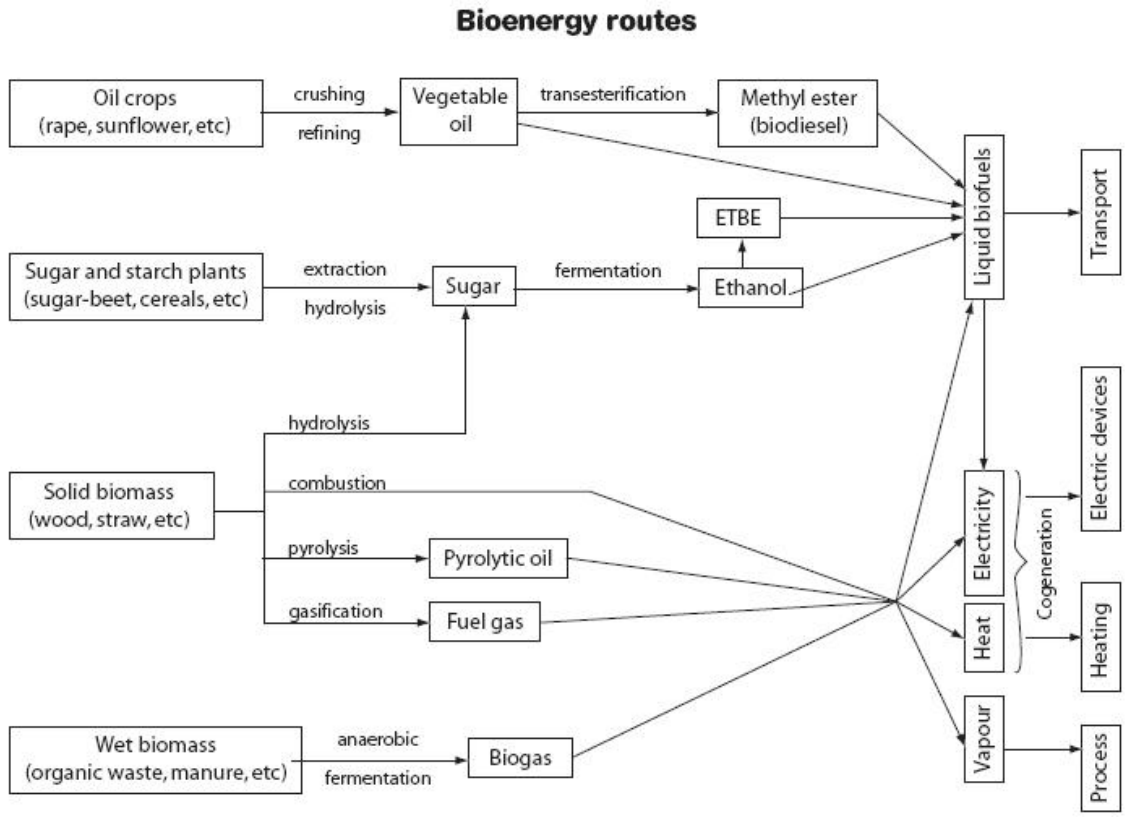

Figure 1.2: Different ways of biomass to bioenergy conversion

1.2 Motivation

Gasification technology exists for a long time but the principles are not yet known. Multiphase fluid dynamics, gas- solid flow, chemical reactions resulting in non-equilibrium state, turbulence and heat transfer, build up a problem unsolved until now. The lack of fundamental understanding of these processes results in empirical structures and correlations based on laboratory experiments and pilot-scale units. Modelling the process via simulation tools will eventually help to design and further on optimize biomass gasifiers of industrial scale. The present thesis is an approach towards this direction.

1.3 Objective of Thesis

At the department of Energy Systems of Technical University of Munich (TUM) a fluidized bed gasifier was built to test various bio fuels. In order to support experimental investigations, a CFD model of the gasifier is developed. The work presented here is dedicated to the simulation of the laboratory scale bubbling fluidised bed reactor. Understanding the fundamentals of the technology and the current knowledge status had to be thoroughly explored in order to successfully handle the problem. A simulation program had to be used in order to achieve up-to-date simulation standards and finally conclude in desired results. The objectives of this thesis are :

- Introduction to the topic
- Review of the existing models for fluidized beds in literature
- Modelling the biomass gasification process
- Validation with experimental data
- Documentation of the results

The work done here, combines the proposed models for the individual processes that have been developed the past years. Experimental testing has taken place in order to compare and validate the model.

1.4 Structure of Thesis

The structure of the study is discussed below :

1. At the first chapter, an introduction is made about the energy demand and the potential of biomass as a sustainable alternative energy source. Then, after a short historical note, the gasification process is defined as well as biomass, and its differences with coal. The chapter ends with the related work so far.

2. At the second chapter, the different types of gasifiers are presented. From type to type, the advantages and disadvantages are discussed. More attention is paid to the fluidized bed gasifier, which is the gasifier studied here.

3. The third chapter analyses the operational characteristics. Bed temperature and the gasifying agent play an important role to the resulting product gas. The gasifier efficiency is then defined and the chapter closes with the Euler-Euler approach which was implemented for the simulation process.

4. The fourth chapter regards the chemical reactions. Drying, primary and secondary pyrolysis, and gasification are further explained. The simulation methods for each step are presented.

5. At the fifth chapter, the fundamentals of the Eulerian model are thoroughly explained. Volume fraction and conservation equations, the kinetic theory of granular flows and complementary models are presented to explain the Eulerian approach.

6. The sixth chapter describes the model which was developed for the simulation process. The reactor's geometry is given along with the phases and materials used. The boundary conditions are defined and the system kinetics follow.

7. Chapter seven finishes with three (3) modelling approaches, their results and discussion.

8. In chapter eight, the prospects for further development are given. The cites and references are included in the Bibliography.

Chapter 2

Principles of gasification

2.1 Historical note

Energy production using the gasification method has been in use for more than 180 years. Initially, peat and coal were used to produce town gas for lighting and cooking in 1800's. While natural gas eventually replaced the need for producer gas, the latter has been in use for production of synthetic chemicals since the 1920's.

During both world wars, especially the Second World War when embargo policies were followed for fuel and petroleum restriction, the need of gasification reemerged. The solution was to use wood gas generators to power motor vehicles in Europe. By 1945 there were trucks, buses and agricultural machines powered by gasification with an estimation of 9,000,000 vehicles running on producer gas all over the world Fig. 2.1,Wikipedia.

Figure 2.1: Adler Diplomat 3 with gas generator (1941)

By the end of the War, oil gained governing position for energy and power production putting aside the producer gas industry. Sweden was the only country to continue research on gasification technology mainly after the 1956 Suez Canal Crisis, including gasifiers in its strategic

emergency plans. Soon after the 1973 oil crisis and the 1979 energy crisis, many countries started dealing again with gasification technology in order to become less dependent on foreign suppliers.

Nowadays, there are many plants producing synthesis gas or co-firing existing coal units. Plants operating on biomass and/or waste include that in Rudersdorf in Germany (500t/d waste) and Geertruidenberg in the Netherlands (400t/d waste wood) using circulating fluid-bed processes. In Rudersdorf the gas is fired in a cement kiln, whereas in Geertruidenberg the hot gas leaving the cyclone at a temperature of about 500 $°C$ is directly co-fired in a 600 MW_e coal boiler (Christopher Higman (2008)).

2.2 Gasification

Gasification is a process that converts organic or fossil-based carbonaceous materials into carbon monoxide, hydrogen, carbon dioxide, methane and nitrogen (if air is used as the oxidizing agent). This is achieved by reacting the material at high temperatures with a controlled amount of air, oxygen or steam. The gas producer, which is called gasifier, is a simple device consisting of a cylindrical container in most applications.

The difference between gasification and combustion is the amount of oxidant supplied. In combustion, the air provided is greater than the stoichiometric ratio needed for complete burning ($\lambda > 1$), when in gasification it is lower with usual values of $\lambda \sim 0.2 - 0.3$. The resulting gas mixture is called syngas, synthesis gas or producer gas and is itself a fuel. The reaction sequence of biomass gasification is shown in Fig. 2.2.

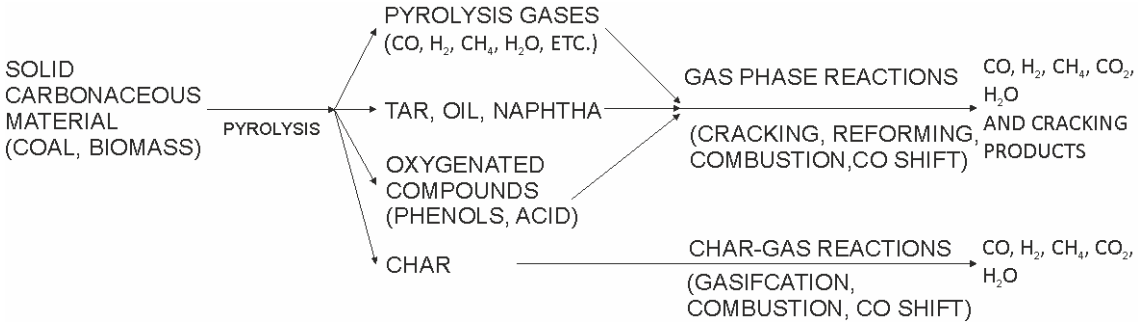

Figure 2.2: Reaction sequence for gasification of coal or biomass (adapted from R. Reimert (1989))

The purpose of gasification modelling is (Christopher Higman (2008)):

1. Calculation of the gas composition

2. Calculation of the relative amounts of oxygen and/or steam and/or heat required per unit fuel intake

3. Optimization of the energy in the form of heat of combustion of the product gas or, alternatively, of the synthesis gas production per unit fuel intake

4. Provision of set points for process control

Syngas can be burned directly in gas engines, internal combustion engines (both compression and ignition), used as a substitute for furnace oil in direct heat applications and can be used to produce, in an economically viable way, methanol as chemical feedstock for industries. It can also be converted via the Fischer-Tropsch process, S.T. Sie (1999) into synthetic fuel.

The conversion process is more complex than combustion, and is influenced by the amount of oxidant, feedstock composition, gasifier temperature, reactor geometry and gas-solid contact. The chemical processes take place at elevated temperatures $> 700\ ^oC$, making a clear difference from biological processes, such as anaerobic fermentation that produce biogas. The advantage of thermochemical over bio-chemical conversion of wood is that lignin is energetically exploited without the need for any special treatment.

The syngas produced is potentially more efficient than direct combustion of the initial fuel because it can be combusted at higher temperatures or even fuel cells. The fuel cells work with electrochemical reaction and so the Carnot's rule for upper limit to the efficiency is not applicable. Another advantage, is that because the fuel input has been converted to gaseous form it is possible to remove the contaminants that cause the emissions prior to combustion. This means drastically reduction of emissions when compared to traditional power plants. Biomass gasification is proved to be a successful option for waste management, chemical production and energy production from non-conventional feeds like forest waste, agricultural waste, poultry waste, municipal refuge and sewage.

The major challenge of gasification technology is to improve control of the product gas composition, which determines the extent of the post-treatment equipment. Tar formation (complex hydrocarbons C_xH_y) can put an investment in great risk. This lack of control is due to the complexity of bed dynamics. Multiphase flow, gas-solid interaction, chemical reactions and turbulence are responsible for the composition of the raw output gas. So far, empirical models and structures have been developed failing to optimize the technology and result in industrial-scale units. For this reason, computational fluid dynamics (CFD) simulations are developed. However, the lack of knowledge in the field of chemical reactions puts a big barrier on the accuracy of the simulation projects.

2.3 Biomass

Biomass is defined as renewable organic matter such as agricultural crops, wood and wood waste, organic components of municipal and industrial waste, or animal waste. It is a natural substance that accumulates solar energy as chemical energy, by the process of photosynthesis, in the presence of sunlight. Biomass fuel is a liquid, solid or gaseous fuel produced by conversion of biomass.

Biomass contains cellulose, hemi-cellulose and lignin, having an average composition of $C_6H_{10}O_5$, with slight variations. For the complete combustion of biomass, the theoretical amount of air required (defined as the stoichiometric quantity) is 6 to 6.5 kg of air per kg of biomass, and the end products are CO_2 and H_2O.

In gasification, biomass is subjected to partial pyrolysis under sub-stoichiometric conditions with the air quantity being limited to 1.5 - 1.8 kg of air per kg of biomass. The resultant mixture of gases generated during the gasification process is called producer gas, contains CO and H_2 and is combustible. The raw producer gas also contains tar and particulate matter which have to be removed when it is used in engine applications.

2.3.1 Biomass analysis

As for coal, the same two types of analyses are followed for biomass in order to determine its burning characteristics. These are the proximate and the ultimate analysis :

Proximate analysis

With proximate analysis the moisture, volatile matter, ash and fixed carbon in the biomass is determined. This method provides an initial indication of the quality and type of biomass. The methods for performing these analyses are standardized by all the major Standard Institutions (ASTM, ISO, DIN, BS etc.).

Moisture is determined first. By drying the biomass sample under standard conditions for 1h at 104-110 $°C$ both the surface moisture and the inherent moisture is released. The inherent moisture is the amount of water that is very loosely bound in biomass.

Volatile matter is determined by heating biomass in a covered crucible for a defined time at a defined temperature in the absence of oxygen. These values differ among the various standards. The loss in mass minus the mass of the moisture, represents the mass of the gaseous constituents formed by the pyrolysis under the conditions mentioned.

Ash is the inorganic residue that remains after combustion of biomass. It consists mainly of salts. Major components of biomass ash are potassium, calcium and phosphorus, and further sodium, magnesium, iron, silicon and trace elements. Biomass ashes have low ash-melting

point of 800 $°C$ for example and are extremely aggressive towards refractory materials, Christopher Higman (2008).

Although the proximate analysis tells a lot about the fuel, the elemental composition of the hydro-carbonaceous part of biomass is also crucial.

Ultimate analysis

At ultimate analysis, the percentages of carbon, hydrogen, oxygen, sulphur and nitrogen are determined. The oxygen percentage, which is relatively high in biomass, gives information about the reactivity of gasification and combustion. Sulphur content is usually low, far under 1% (wt% dry). The biomass-derived nitrogen is the reason why it is not essential to gasify biomass with ultra-pure oxygen, even when the gas is used for hydrogen production.

Typical data for some vegetable biomasses are included in Tables 2.1, and 2.2, Christopher Higman (2008):

2.3.2 Differences between coal and biomass gasification

Even though coal gasification is often exploited to model biomass gasification, there are some basic differences between coal and biomass. Biomass is more reactive because of the high oxygen percentage ($\sim 45\%$). It pyrolyzes fast, has more volatile and moisture, less energy density, little ash and sulfur content. Furthermore, vegetable biomass has fibrous characteristics. For these reasons another solid called fluidizing, has to be used in the gasifier and it is usually silica sand or olivine.

These differences make clear the need of a detailed model specifically for biomass gasification. However, comprehensive and advanced models for biomass gasification in fluidized beds are scarce in literature Alvaro Sanz (2005); D. Lathouwers (2001a); Michael Oevermann (2009); Priyanka Kaushal (2010); S. Gerber (2010).

2.3.3 Emissions

With energy supplied from biomass as a renewable source, there is almost no net CO_2 emission, as the CO_2 released to the atmosphere will be taken up by plants in a relatively short time scale. By substitution of coal or other solid fossil fuels by biomass, net CO_2 emissions will be reduced to a significant extent. Furthermore, if the fossil fuels used for biomass production, transportation, conversion and distribution were replaced by biomass, it would be possible to reduce or even eliminate net CO_2 emissions.

The emissions of SO_2 are lower to coal-fire plants because the sulfur content in biomass is very low. In addition, the thermal NO_x emissions are negligible due to low operating temperatures.

Table 2.1: Properties of various biomasses

Biomass	**HHV (MJ/kg)**	**Moisture (wt%)**	**Ash (wt%)**	**Sulphur (wt%)**	**Chlorine (wt% dry)**
Charcoal	25-32	1-10	0.5-6		
Wood	10-20	10-60	0.25-1.7	0.01	0.01
Coconut shell	18-19	8-10	1-4		
Straw	14-16	10	4-5	0.07	0.49
Ground nut shells	17	2-3	10		
Coffee husks	16	10	0.6		
Cotton residues (stalks)	16	10-20	0.1		
Cocoa husks	13-16	7-9	7-14		
Palm oil residues (shells)	15	15			
Rice husk	13-14	9-15	15-20		
Soya straw	15-16	8-9	5-6		
Cotton residue (gin trash)	14	9	12		
Maize (stalk)	13-15	10-20	2(3-7)	0.05	1.48
Palm oil residues (fibres)	11	40			
Sawdust	11	35	2		
Bagasse	8-10	40-60	1-4		
Palm oil residues (fruit stems)	5	63	5		
Bark				0.7	0.49

Table 2.2: Analysis of typical biomass

Proximate analysis			**Ultimate analysis**	
Volatile matter	wt% maf	>70	C, wt%	54.7
Ash	wt% ar	1.5	H, wt%	6.0
Moisture	wt% ar	20	O, wt%	38.9
Fixed carbon	wt% ar	<15	N, wt%	0.3
			S, wt%	0.1

2.4 Types of gasifiers

There are many types of gasifiers ranging from simple to more complicated geometries. The need for different structures has occurred in order to handle the remaining ash or to minimize the production of tar inside the producer gas. Tar is a major problem because when condensed it sticks to the walls of the downstream equipment.

The reactor of the gasification plant is called gasifier and can take one of the following forms Prabir Basu (2009) :

1. Fixed bed gasifier (Up-draft, Down-draft, Side-draft)
2. Fluidized bed gasifier (bubbling bed, circulating fluidized bed, spout fluid bed)
3. Entrained bed

The schematics of the above structures are shown in Fig. 2.3 Prabir Basu (2009).

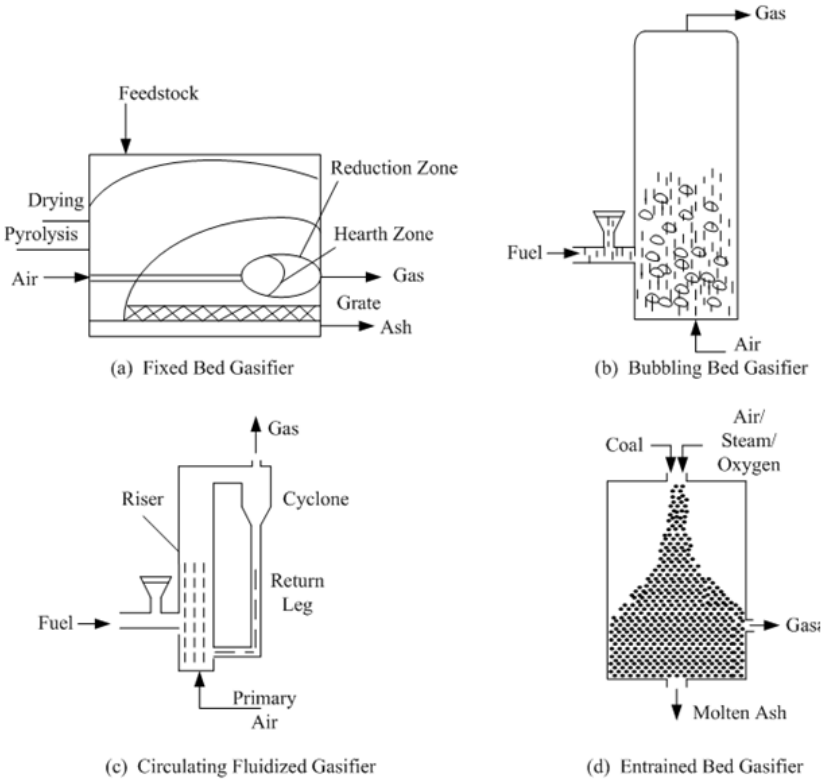

Figure 2.3: Different types of gasifiers

2.4.1 Up-draft or counter current gasifier

The up-draft gasifier consists of a fixed bed with carbonaceous fuel (e.g. coal or biomass) through which the gasification agent (steam, oxygen, air or carbon dioxide) flows in counter-current configuration. The ash produced is either removed dry, or as a slag, depending on the working

temperature. Thermal efficiency is high because the gas exit temperatures are relatively low. This means that tar and methane production is significant and the producer gas needs to be cleaned before use.

The counter current or up-draft gasifier is the oldest and simplest type of gasifier, shown in Fig.2.4, FAO. The air intake is at the bottom and the gas leaves at the top. Near the grate at the bottom the combustion reactions occur, which are followed by reduction reactions somewhat higher up in the gasifier. In the upper part of the gasifier, heating and pyrolysis of the feedstock occur, as a result of heat transfer by forced convection and radiation from the lower zones. The tars and volatiles produced during this process will be carried in the gas stream. Ashes are removed from the bottom of the gasifier.

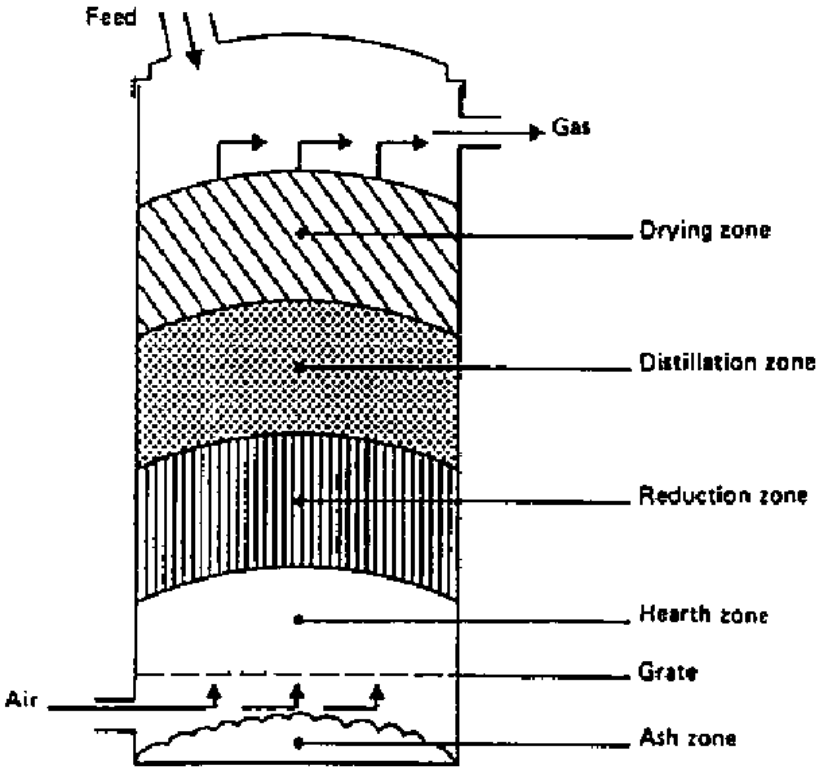

Figure 2.4: Up-draft gasifier

The major advantages of this type of gasifier are its simplicity, high charcoal burn-out and internal heat exchange leading to low gas exit temperatures and high equipment efficiency, as well as the possibility of operation with many types of feedstock (sawdust, cereal hulls, etc.).

Major drawbacks derive from the possibility of channelling [1] in the equipment. Channelling can lead to oxygen break-through and dangerous, explosive situations and the necessity to install automatic moving grates, as well as from the problems associated with disposal of the

[1] Channelling is an operational problem. Air is not uniformly distributed through the gasifier but follows low-pressure channels. This can result from insufficient air supply or packed bed conditions.

tar-containing condensates that derive from the gas cleaning operations. The latter is of minor importance if the gas is used for direct heat applications, in which case the tars are simply burnt. Due to the high tar content of the producer gas (up to 150 g/m^3), updraft gasifiers are not suitable for engines and gas turbines without comprehensive gas cleaning C. Mandl (June/July 2009).

2.4.2 Down-draft or co-current gasifier

The down-draft gasifier is similar to the counter-current type, but the gasification agent flows in co-current configuration with the fuel. This structure elevates the exiting temperature of the producer gas, helping tar cracking so that tar levels are much lower than in counter-current. The producer gas is removed at the bottom of the apparatus, so that fuel and gas move in the same direction, as schematically shown in Fig. 2.5, FAO.

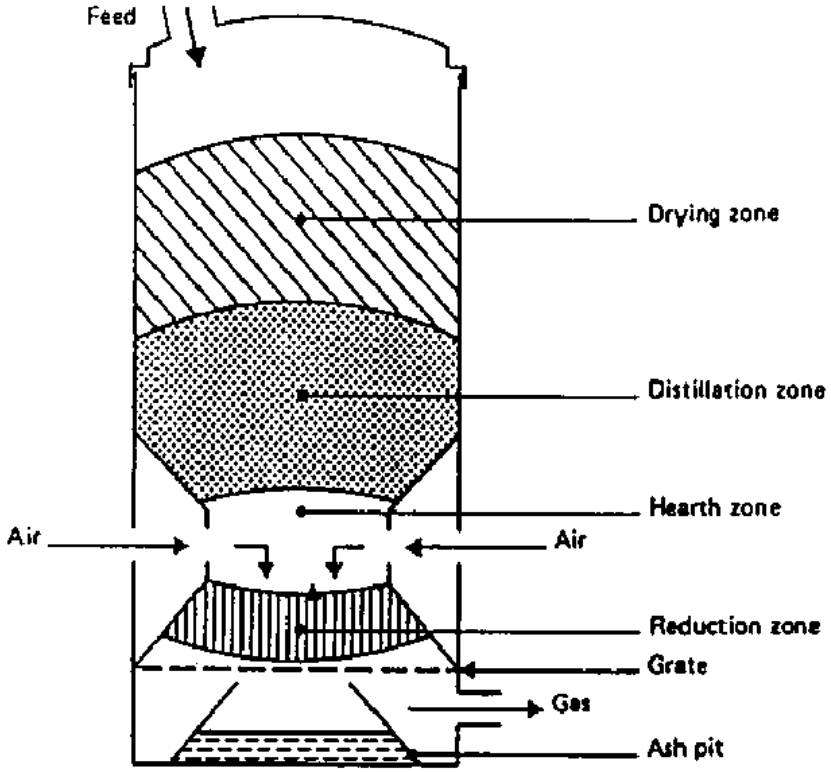

Figure 2.5: Down-draft gasifier

On their way down, the acid and tarry distillation products from the fuel must pass through a glowing bed of charcoal and therefore are converted into permanent gases, such as hydrogen, carbon dioxide, carbon monoxide and methane. Depending on the temperature of the hot zone and the residence time of the tarry vapours, a more or less complete breakdown of the tars is achieved. The main advantage of down-draft gasifiers lies in the possibility of producing a tar-free gas, suitable for engine applications. Because of the lower level of organic components in the condensate, down-draft gasifiers suffer less from environmental objections than up-draft gasifiers.

In practice, however, a tar-free gas is seldom if ever achieved over the whole operating range of the equipment: tar-free operating turn-down ratios of a factor 3 are considered standard; a factor 5-6 is considered excellent.

A major drawback of down-draft equipment, lies in its inability to operate on a number of unprocessed fuels. In particular, fluffy, low density materials give rise to flow problems and excessive pressure drop, and the solid fuel must be pelletized or briquetted before use. Down-draft gasifiers also suffer from the problems associated with high ash content fuels (slagging) to a larger extent than up-draft gasifiers. Minor drawbacks of the down-draft system, as compared to up-draft, are somewhat lower efficiency resulting from the lack of internal heat exchange as well as the lower heating value of the gas. Besides this, the necessity to maintain uniform high temperatures over a given cross-sectional area makes impractical the use of down-draft gasifiers in a power range above about 350 kW (shaft power).

2.4.3 Cross-draft gasifier

Cross-draft gasifiers, schematically illustrated in Fig. 2.6, FAO are an adaptation for the use of charcoal. Charcoal gasification results in very high temperatures (1,500 $^{\circ}C$ and higher) in the oxidation zone which can lead to material problems. In cross draft gasifiers, insulation against these high temperatures is provided by the fuel (charcoal) itself.

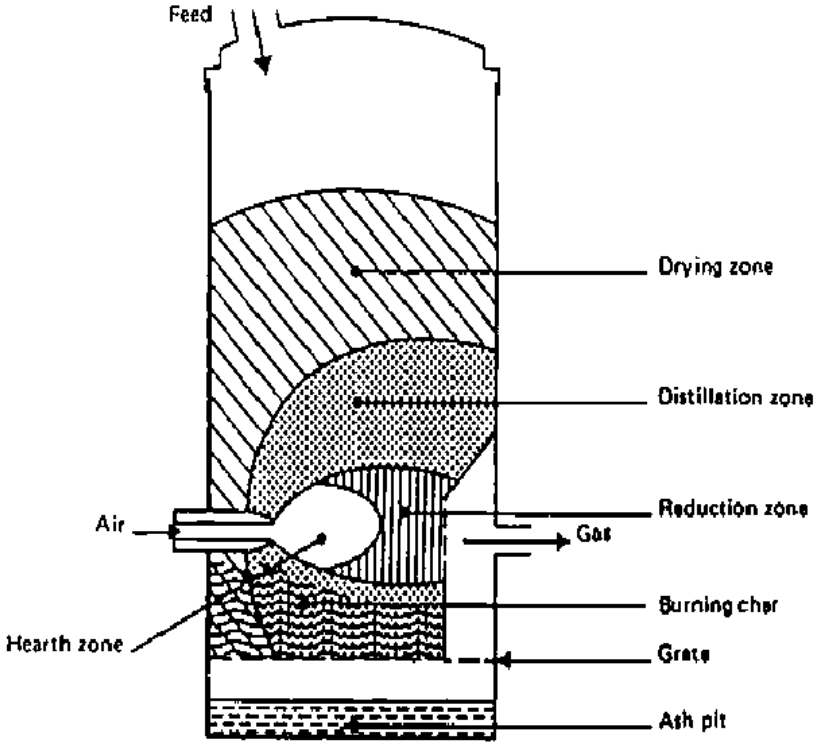

Figure 2.6: Cross-draft gasifier

Advantages of the system lie in the very small scale at which it can be operated. Installations below 10 kW (shaft power) can, under certain conditions, be economically feasible. The reason is the very simple gas-cleaning train (only a cyclone and a hot filter) which can be employed when using this type of gasifier in conjunction with small engines.

A disadvantage of cross-draft gasifiers is their minimal tar-converting capabilities and the consequent need for high quality (low volatile content) charcoal. It is because of the uncertainty of charcoal quality, that a number of charcoal gasifiers employ the down-draft principle, in order to maintain at least a minimal tar-cracking capability.

2.4.4 Fluidized bed gasifier

The operation of both up and down-draft gasifiers is influenced by the morphological, physical and chemical properties of the fuel. Problems commonly encountered are: lack of bunkerflow, slagging and extreme pressure drop over the gasifier. A design approach aiming at the removal of the above difficulties is the fluidized bed gasifier illustrated schematically in Fig. 2.7, FAO.

In a fluidized bed gasifier the granular inert solids (usually silica sand) along with the feedstock are fluidized by the gasifying agent. The fluidization principle is simple. Passing a fluid upwards through a packed bed of solids produces a pressure drop due to fluid drag. When the fluid drag is equal to the bed weight, the particles no longer rest on each other, resembling a fluid's motion. The minimum fluidising velocity is denoted as U_{mf}, showing the minimum velocity of the fluid for which the bed gets into fluidized state. Gasification is an endothermic process, so internal or external heat is needed to sustain the process. The working temperature is usually 800-950^oC.

Fluidized bed gasifiers are most useful for fuels that form highly corrosive ash, that would damage the walls of slagging gasifiers. Biomass fuels generally contain high levels of corrosive ash. The production of wood gas in fluidized bed reactors is regarded as one of the most promising techniques to efficiently exploit the energy from biomass.

Air is blown through a bed of solid particles at a sufficient velocity to keep these in a state of suspension. The bed is originally externally heated and the feedstock is introduced as soon as a sufficiently high temperature is reached. The fuel particles are introduced at the bottom of the reactor, very quickly mixed with the bed material and almost instantaneously heated up to the bed temperature. As a result of this treatment, the fuel is pyrolysed very fast, resulting in a component mix with a relatively large amount of gaseous materials. Further gasification and tar-conversion reactions occur in the gas phase. Most systems are equipped with an internal cyclone in order to minimize char blow-out as much as possible. Ash particles are also carried over the top of the reactor and have to be removed from the gas stream if the gas is used in engine applications.

The major advantages of fluidized bed gasifiers stem from their feedstock flexibility to easily control the temperature, which can be kept below the melting or fusion point of the ash (rice

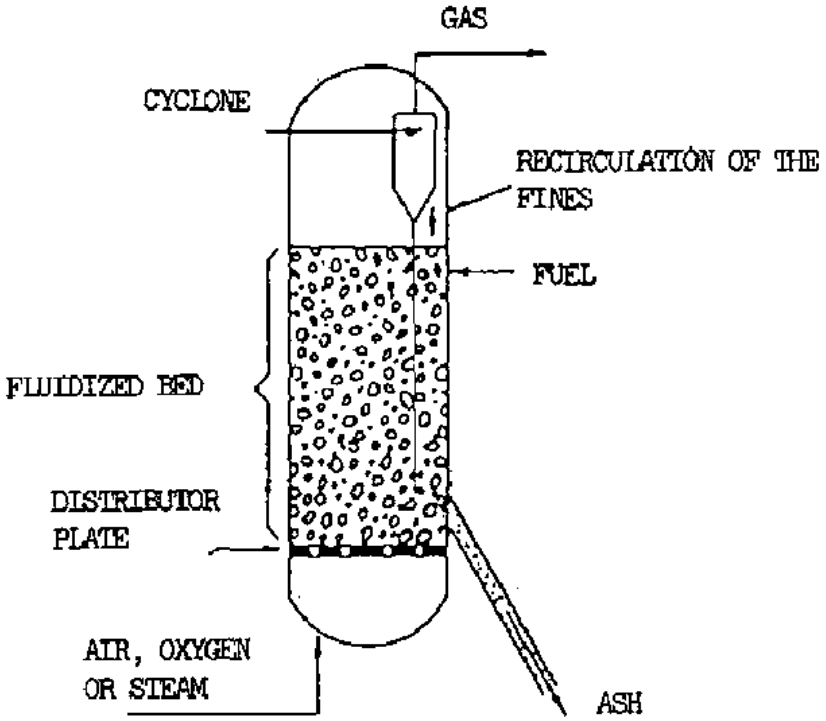

Figure 2.7: Fluidized bed gasifier

husks), and their ability to deal with fluffy and fine grained materials (sawdust etc.), without the need of pre-processing. Problems with feeding, instability of the bed and fly-ash sintering in the gas channels can occur with some biomass fuels FAO.

Drawbacks of the fluidized bed gasifier lie in the rather high tar content of the product gas (up to 500 mg/m^3 gas), the incomplete carbon burn-out, and poor response to load changes.

Particularly because of the control equipment needed to cater for the latter difficulty, very small fluidized bed gasifiers are not foreseen and the application range must be tentatively set at above 500 kW (shaft power). Fluidized bed gasifiers are currently available on a semi-commercial basis from several manufacturers in Europe and the U.S.A.

2.4.5 Other types of gasifiers

Entrained flow gasifiers

In entrained flow gasifiers, Fig.2.3, a dry pulverized solid, an atomized liquid fuel or a fuel slurry is gasified with oxygen (less frequent with air) in co-current flow. The gasification reactions take place in a dense cloud of very fine particles. High temperatures are achieved so that tar and methane are not present in the producer gas, but the need for oxygen as gasifying agent is cost intensive. The major part of the ash is removed as a slag because the operating temperature

is above the ash fusion temperature. Entrained-flow gasifiers have become the preferred gasifier for hard coals, and have been selected for the majority of commercial-sized IGCC applications Christopher Higman (2008).

A number of other biomass gasifier systems (double fired, molten bath), which are partly spin-offs from coal gasification technology, are currently under development. In some cases these systems incorporate unnecessary refinements and complications, in others both the size and sophistication of the equipment make near term application in developing countries unlikely. For these reasons they are omitted from further discussion in this study.

Chapter 3

Operational characteristics

3.1 Bed temperature

The bed's temperature has a crucial impact on the whole procedure and the products in all ways. It determines the equilibrium composition of the gas. Biomass ash has a melting point of approximately 1.000^oC. Thus, it is important to keep the operating temperature below this level in order to avoid ash sintering and slagging. The bed's highest temperature is limited by char agglomeration as well. This happens when the reaction rates are low and the overall gasification efficiency falls because part of the fuel remains in unconverted char mode. As it has been observed from the lab-scale gasifier, unreacted char particles can reach very high heating values of 30 MJ/kg, when the initial feed has 20 MJ/kg.

On the other hand, the gasifier temperatures should be sufficiently high to produce non-condensable tars in order to avoid problems in downstream conversion equipment. If the product gas is used in engine or gas turbine applications rather than direct heating, tars must be cracked or removed a priori. This is why tar formation in the product gas can make the process unsuitable from a technical and economical point of view, as mentioned in A. Gómez-Barea (2010).

The usual temperature that combines all benefits is around 800^oC. This is the temperature achieved and measured at the present experimental structure. The gasification chemical reactions sum up at endothermal state inside the reactor. So, the surplus heat has to be given from another source. There are autothermal and allothermal processes for heat support depending on the gasifying agent.

3.1.1 Autothermal and allothermal heating

Autothermal heating takes place when the oxidant is air or oxygen and the heat can be obtained from partial oxidation of the fuel inside the reactor. On the other hand, allothermal heating takes place when steam is used as oxidant and heat has to be given externally.

In the current study, steam is used as oxidant, and several allothermal processes are discussed below. The two main concepts in order to solve the heat transfer problem are either to circulate hot solids (i.e. fluidized bed material) from a combustion zone (e.g. Batelle gasifier, Gussing gasifier etc.), or to use indirectly heated fluidized bed gasifier systems, with integrated heat exchanger tubes S. Karellas (2008).

Other ideas are to expose the reactor to concentrated solar radiation and use carbonaceous compounds only for the gasification. Z'Graggen and Steinfeld A. Z' Graggen (2008) proposed a reactor directly exposed to concentrated solar radiation. By this way, the external energy used for the gasifier's operation is less (only during night), reducing the total CO_2 emissions.In this case, the initial capital cost increases, as well as the maintenance cost for the moving parts of the mirrors used. Very high temperature nuclear reactors can achieve the same, avoiding the source availability and the fluctuation of solar radiation. Gordillo and Belghit E.D. Gordillo (2011), used hot steam from a nuclear reactor as the sole energy source. The technology of nuclear energy is fully understood but the safety issues are always vital.

Here the heat transfer is accomplished via four electric heated heatpipes inside the reactor at the level of the sand. Further discussion on the topic is made at section 6.5.

3.2 The gasifying agent

When the gasifying agent is air, the process is named air gasification and the producer gas has lower quality in terms of heating value (LHV$\sim$ 4-7 MJ/Nm^3) due to the high percentage of nitrogen mixed inside the gas. This gas is suitable for boilers, engines and turbines.

If the gasifying agent is pure oxygen or steam, it is called oxygen or steam gasification respectively. In this case the producer gas has relatively high quality (LHV$\sim$ 10-18 MJ/Nm^3) and can be used for conversion to methanol and gasoline G. Schuster (2001) .

Gasification with pure O_2 is not practical due to prohibitively high costs for O_2 production using current commercial technology. So steam gasification was modelled in this study. The advantages of steam gasification are maximum hydrogen production, efficient tar reduction and higher char conversion C. Franco (2002); C. Lucas (2004).

It is common to express the extent of steam addition, as steam to biomass ratio (STBR) :

$$STBR = \frac{Steam + Fuelmoisture(kg/s)}{Drybiomass(kg/s)} \tag{3.1}$$

The minimum value for steam to biomass ratio must be $STBR_{min} \approx 0.4$, in order to complete carbon conversion into gaseous compounds, as it is predicted from thermodynamics.

3.3 Gasifier efficiency

An important factor that determines the actual technical operation, as well as the economic feasibility of using a gasifier system, is the gasification efficiency.

When the gas is used for engine applications, the efficiency is defined as :

$$\eta_m = \frac{H_g \cdot Q_g}{LHV_s \cdot M_s} \cdot 100(\%) \tag{3.2}$$

where
η_m = gasification efficiency % (mechanical)
H_g = heating value of the gas (kJ/m^3)
Q_g = volume flow of the gas (m^3/s)
LHV_s = lower heating value of gasifier fuel (kJ/kg)
M_s = gasifier solid fuel consumption (kg/s)

If the gas is used for direct burning, the gasification efficiency is defined as :

$$\eta_{th} = \frac{(H_g \cdot Q_g) + (Q_g \cdot \rho_g \cdot C_p \cdot \Delta T)}{LHV_s \cdot M_s} \cdot 100(\%) \tag{3.3}$$

where
η_{th} = the gasification efficiency % (thermal)
ρ_g = the density of the gas (kg/m^3)
C_p = the specific heat of the gas (kJ/kgK)
ΔT = temperature difference between the gas at the burner inlet and the fuel entering the gasifier (K).

Normal values for η_m are 60-75 % depending on the type and design of the gasifier and 93 % for η_{th}, for the cases of thermal applications FAO.

Chapter 4

Chemical Processes

The gasification process can be further separated into the following steps :

1. Drying
2. Pyrolysis
3. Char gasification and char oxidation

Char oxidation supplies part of the heat required by the endothermic gasification reactions.

4.1 Drying

Once the feed enters the gasifier it is heated up and dried, releasing water until about 200^oC. After 100^oC, the superficial water from biomass is irreversibly removed. Then, the inherent moisture inside the biomass particles is released. During this process, the volatiles start to release as well. This is why, it is a common practice to couple drying with pyrolysis, as the two procedures overlap.

Drying is orders of magnitude faster than any of the gasification reactions taking place inside the gasifier. For this reason, at the present work, the fuel's moisture is instantaneously released at the point of the feed. This is simulated as a chemical reaction in which the solid's water is transferred to the water specie of the gas phase, with very fast Arrhenius kinetic rate parameters (see section 6.7):

$$H_2O_{solid} \longrightarrow H_2O_{gas}$$

4.2 Pyrolysis

4.2.1 Primary pyrolysis

Primary pyrolysis is the initial thermochemical decomposition of organic material at elevated temperatures, in the absence of oxygen. It is sometimes referred to as devolatilization. These terms will be used synonymously in this thesis, even though the technical difference between the two is whether or not the thermal decomposition of the particle takes place in the absence

(pyrolysis) or presence (devolatilization) of oxygen.

Primary pyrolysis takes place when the dried fuel is heated in the range of 200-500^oC and decomposes into permanent gases, condensable vapor - tar, and solid residue - char. Each of these products is a complex mixture of different species. The actual composition of wood gas and tar strongly depend on the heating rate, Blasi (2008); Christopher Higman (2008), and the heating temperature Gronli (1996).

If the heating rate is slow, pyrolysis starts from 350$^\circ C$. The gasification reaction of both volatiles and char with steam are very slow at this temperature. The concentration of volatiles outside the particle increases rapidly, and gasification only sets in after devolatilization is complete. However, if the heating rate is high, then both pyrolysis and gasification take place simultaneously, so that high concentration of volatiles is never allowed to build up, Christopher Higman (2008).

A high tar yield can be desirable (e.g. production of pyrolysis oil) or undesirable (e.g. production of gas for gas engines), but in any case knowledge of the cracking kinetics is of major importance for finding optimal operating conditions and an optimal reactor design, J. Rath (2001).

It is important in modelling to know the relative amounts of the devolatilization products (i.e., gas, tar, and char) because these products are then used in the gasification and partial combustion and determine the final composition of the product gas. Thus, the knowledge of kinetic and transport phenomena that characterize the reactor is essential to design and optimize the pyrolysis process, in order to achieve industrial application.

An overview of the available pyrolysis models with an extended literature survey can be found in the review of Blasi (2008). Some elaborated pyrolysis models use particle data in the context of Euler-Lagrange approach and can't be used in Euler-Euler models (for differences see section 4.5.1).

Gronli (1996) proposed a model for primary pyrolysis which has been later on used from J. Larfeldt (2000) and S. Gerber (2010), assuming a reaction path:

$$\text{wood} \longrightarrow \text{wood gas}(H_2O, CO, CO_2, H_2, CH_4) + \text{char} + \text{tar}$$

The composition of wood gas, resulting from the primary pyrolysis step, is strongly dependent from the heating rate, the heating temperature and the nature of the wood used. The actual composition and the reaction rates of a feed can be found only after specific experimental research.

Tar is a complex mixture of different components, mainly Polycyclic Aromatic Hydrocarbons (PAH) like naphthalene, phenanthrene and anthracene. Their general chemical form is C_xH_y and little is known about the exact chemical reactions leading to such complex formations. For

these reasons, tar, as well as inert tar, was not taken into consideration in the current work.

The char product is assumed to consist of pure carbon, which is the usual simulation method found in literature. It is simulated as a single solid phase with a constant diameter.

4.2.2 Secondary pyrolysis

Secondary pyrolysis refers to processes such as cracking, polymerization, condensation, or carbon deposition that result from the reaction of the primary pyrolysis products at high temperatures and sufficiently long residence times, Smoot L.Douglas (1985).These reactions occur homogeneously in the gas phase and heterogeneously at the surface of the solid fuel or char particles, J.C. Wurzenberger (2002). Exposing wood tar to high temperatures at long residence times causes most of the tar to crack into light gas. The whole amount of these gases would be detected if the reactor was operated as a pyrolizer, with an inert gas agent.

Numerous factors affect the pyrolysis rate and the yields, composition and properties of the product gas. Temperature, pressure, heating rate and biomass properties, such as chemical composition, ash content and composition, particle size and shape, density and moisture content are the major ones. C. A. Koufopanos (1989) proposed a universal method of modelling biomass pyrolysis considering it as a sum of its main components, namely cellulose, hemicellulose, and lignin.

The model of M.J. Boroson (1989) assumes that the tar from the primary pyrolysis step decomposes giving wood gas via reactive tar_1 and inert tar :

$$\text{tar} \longrightarrow tar_1 + tar_{inert} \longrightarrow \text{woodgas}(H_2O, CO, CO_2, H_2, CH_4) + tar_{inert}$$

The proportion of the inert tar differs among the existing models. It is clearly understood that the exact amount of inert tar is temperature dependent, as every aromatic substance would crack in higher temperatures. Other models propose two reactive tar components with different reaction rates. The final product of secondary pyrolysis is assumed to include H_2O, CO, CO_2, H_2 and CH_4 in most engineering applications ignoring possible C_2H_4, C_2H_6, C_3H_6, C_2H_2 mass fractions as negligible amounts.

4.3 Char-gas interaction

Gasification is the process by which any carbonaceous species can be converted into a gaseous fuel called syngas through partial oxidation, as already discussed in 2.2. This process takes place at temperatures in the range 800-1800^oC, Christopher Higman (2008). The exact temperature depends on the characteristics of the feedstock, in particular the softening and melting temperatures of the ash.

The char remaining from the pyrolysis step is considered to consist of pure carbon and undergoes some heterogeneous reactions to produce part of the product gas. The reactions mostly used for this reason are the following :

1. Partial oxidation of char : $C + \frac{1}{2}O_2 \rightarrow CO$ -111 MJ/Kmol

2. Boudouard reaction : $C + CO_2 \rightarrow 2CO$ +172 MJ/Kmol

3. Heterogeneous Water-gas reaction : $C + H_2O \rightarrow CO + H_2$ +131 MJ/Kmol

4.4 Gas-gas reactions

Except for the heterogeneous reactions, there are also homogeneous at the gas phase. The two most important reactions are presented here :

1. Water-gas shift reaction : $CO + H_2O \leftrightarrows CO_2 + H_2$ -41 MJ/kmol

2. Steam methane reforming reaction : $CH_4 + H_2O \leftrightarrows CO + 3H_2$ +206 MJ/kmol

4.5 Literature review

Many researchers have contributed into creating models that analyze gasification procedures. The published work concerning biomass gasification is scarce compared to coal gasification and most of the time, the models concerning coal are fitted to biomass, only by changing the fuel's composition. This is mainly because coal and biomass have the same chemical components, just in different analogies.

4.5.1 Modelling approaches

Two major modelling approaches can be identified. The first one is the Euler-Lagrange approach. Here, the trajectory and state (temperature, mass, composition and velocity) of each individual solid-phase particle is tracked in space and time, by integrating the equations of motion, energy and mass for each particle. The modelling accuracy resulting from individual scale analysis is accompanied with computational cost, proportional to the number of solid particles. Thus, when modelling dense fluidized beds, where the number of solids is of an order of magnitude of trillion, the use of Euler-Lagrange becomes impractical.

The second modelling approach is Euler-Euler. With this model the particulate phase is considered as a continuous phase interpenetrating and interacting with the gas phase. The kinetic theory of granular flows ,J. Ding (1990), is used to derive the equations for the solid phases and

the gas-particle interactions. This approach requires lower computational resources and calculation times. It also allows a detailed analysis of the dispersed phase flow field, which is acceptable for engineering design applications. Some indicative research with model parameters of both modelling approaches and results is presented below.

D. Sofialidis (2001), investigated biomass gasification in a bubbling fluidized bed. The inert sand bed was modelled as a static isotropic porous media containing prescribed spherical volumes to model the presence of rising bubbles. The biomass particles were modelled as Lagrangian particles. The model takes into account drying and devolatilization of biomass, heterogeneous reactions of char, and a single reaction in the gas phase converting water and methane into carbon monoxide and hydrogen. The simulated exhaust gas concentrations of a 3D gasifier agree reasonably well with measured data for H_2, O_2, CO_2, and H_2O, but underpredict CO_2 and overpredict CO concentrations.

D. Lathouwers (2001a,b) used an Euler-Euler approach for the simulation of biomass pyrolysis in a dense fluidized bed of a laboratory scale reactor. Solid phases for biomass, an active intermediate, char, and inert sand particles are introduced with a simple pyrolysis model. Qualitative results for tar yields under different operating conditions are reported. Within the presented simulation times of 5 s, a steady state is not reached and comparisons with experimental data are not included in the study. The focus of the study is on optimizing tar yields from pyrolysis, and results of products other than tar are not included.

Liang Yu (2007) used the kinetic theory of granular flow to simulate coal gasification in a bubbling fluidised bed gasifier. The model considers instantaneous drying and devolatilization in the feed zone with proportion of products distribution, resulting from experiments. Char is modelled as a single solid phase with constant diameter, and heterogeneous reactions are included as well as heterogeneous gas reactions. Different cases for coal feeding rate, air supply, steam supply, and temperature are investigated with good agreement between experimental and simulation results.

K. Papadikis (2008) used continuous Euler-Euler approach to model the behaviour of the sand, and Euler-Lagrange for the investigation of momentum transport to one biomass particle inside the reactor. The simulation lasted for 3 seconds and the work focused mainly on the fluidization behaviour.

S. Gerber (2010) presented an Eulerian multiphase approach for modelling the gasification of wood in bubbling fluidised beds, using char as bed material. Their results were validated with experimental data of a laboratory scale fluidised bed, but their kinetic model was not able to handle general multi-component biomass simulations.

In an other work, Michael Oevermann (2009) presented an Euler-Lagrange / Discrete Element Method (DEM) modelling approach for the simulation of wood gasification in a bubbling fluidized bed in a quasi two-dimensional setting. The soft-sphere collision model was used and pyrolysis,

heterogeneous gasification reactions, and homogeneous gas reactions were considered. Although reasonable agreement between the experiments and the simulation was achieved, it is concluded that a fully three-dimensional Euler-Lagrange simulation of a chemically reacting gas-solid flow for a real size reactor is computationally very demanding. They assumed a heat-neutral pyrolysis step and neglected inert tar.

Concluding, the models developed for biomass gasification in fluidized beds are scarce and take into account different approaches and assumptions. Three-dimensional models considering drying, pyrolysis, gasification, heat transfer, turbulence and chemical reactions within the framework of commercial Fluid Dynamics (CFD) codes are even fewer. The present work hopes to contribute towards this direction.

Chapter 5

Eulerian Model

5.1 Overview of the Eulerian Model

The Eulerian multiphase model in Ansys Fluent, allows for the modelling of multiple separate, yet interacting phases. The phases can be liquids, gases, or solids in any combination. An Eulerian treatment is used for each phase, in contrast to the Eulerian-Lagrangian treatment that is used for the discrete phase model.

With the Eulerian multiphase model, the number of secondary phases is limited only by memory requirements and convergence behavior. Any number of secondary phases can be modeled, provided that sufficient memory is available.

The Eulerian multiphase model does not distinguish between fluid-fluid and fluid-solid (granular) multiphase flows. A granular flow is simply one that involves at least one phase that has been designated as a granular phase. A single pressure is shared by all phases and momentum and continuity equations are solved for each of them. The kinetic theory of granular flow is applied for the conservation of the solid's fluctuation energy. The algebraic formulation was used for the specification of the granular temperature, as presented in the following sections.

Solid-phase shear and bulk viscosities are obtained by applying kinetic theory to granular flows. Frictional viscosity, for modelling granular flow, and several interphase drag coefficient functions are available in the program.

5.2 Volume Fraction Equation

The description of multiphase flow as interpenetrating continua incorporates the concept of phasic volume fractions, denoted here by α_q. Volume fractions represent the space occupied by each phase, and the laws of conservation of mass and momentum are satisfied by each phase individually.

The derivation of the conservation equations can be done by ensemble averaging the local instantaneous balance, for each of the phases, T. B. Anderson (1967), or by using the mixture theory approach, Bowen (1967).

The volume of phase q, V_q, is defined by :

$$V_q = \int \nu \alpha_q \, dV \tag{5.1}$$

where

$$\sum_{q=1}^{n} \alpha_q = 1 \tag{5.2}$$

The effective density of phase q is :

$$\overline{\rho}_q = \alpha_q \rho_q \tag{5.3}$$

where ρ_q is the physical density of phase q.

The volume fraction equation may be solved either through implicit or explicit time discretization. In this study the Implicit Scheme was implemented.

5.3 The Implicit Scheme

When the implicit scheme is used for time discretization, standard finite-difference interpolation schemes, QUICK, Second Order Upwind and First Order Upwind, and the Modified HRIC schemes, are used to obtain the face fluxes for all cells, including those near the interface.

$$\frac{a_q^{n+1}\rho_q^{n+1} - a_q^n \rho_q^n}{\Delta t} V + \sum f \left(\rho_q^{n+1} U_f^{n+1} a_{q,f}^{n+1} \right) = \left[S_{aq} + \sum_{p=1}^{n} (\dot{m}_{pq} - \dot{m}_{qp}) \right] V \tag{5.4}$$

Since this equation requires the volume fraction values at the current time step (rather than at the previous step, as for the explicit scheme), a standard scalar transport equation is solved iteratively for each of the secondary-phase volume fractions, at each time step.

The implicit scheme can be used for both time-dependent and steady-state calculations.

5.4 Conservation of Mass

Eulerian continuum modelling is the most common used approach for fluidised bed simulations. The accumulation of mass in each phase is balanced by the convective mass fluxes. The phases are able to interpenetrate, but the sum of all volume fractions in each computational cell is unity.

The continuity equation for phase q, is in general :

$$\frac{\partial}{\partial t}(\alpha_q \rho_q) + \nabla \cdot (\alpha_q \rho_q \overrightarrow{\nu}_q) = \sum_{p=1}^{n} (\dot{m}_{pq} - \dot{m}_{qp}) + S_q \tag{5.5}$$

where $\overrightarrow{\nu}_q$ is the velocity of phase q , $\dot{m}_{qp}$ characterizes the mass transfer from phase q to phase p, and S_q describes the source term.

The right-hand side of Equation (5.5) is zero. This is because the net mass transfer from one phase to another is zero [1], and the source term is considered by default zero except for the constant user-defined boundary conditions. So, we have the following continuity equations :

Gas phase :

$$\frac{\partial}{\partial t}(\alpha_g \rho_g) + \nabla \cdot (\alpha_g \rho_g \overrightarrow{\nu}_g) = 0 \tag{5.6}$$

Solid phase :

$$\frac{\partial}{\partial t}(\alpha_s \rho_s) + \nabla \cdot (\alpha_s \rho_s \overrightarrow{\nu}_s) = 0 \tag{5.7}$$

5.5 Conservation of Momentum

Newton's second law of motion states that the change in momentum equals the sum of forces on the domain.

The momentum balance for phase q yields in general :

[1] the transfer of mass between phases is considered through reaction kinetics rather than net mass transfer

$$\frac{\partial}{\partial t}(\alpha_q \rho_q \overrightarrow{\nu}_q) + \nabla \cdot (\alpha_q \rho_q \overrightarrow{\nu}_q \overrightarrow{\nu}_q) = -\alpha_q \nabla p + \nabla \cdot \overline{\overline{\tau_q}} + \alpha_q \rho_q \overrightarrow{g} + \sum_{p=1}^{n} \left(\overrightarrow{R}_{pq} + \dot{m}_{pq} \overrightarrow{\nu}_{pq} - \dot{m}_{qp} \overrightarrow{\nu}_{qp} \right) + \left(\overrightarrow{F}_q + \overrightarrow{F}_{lift,q} + \overrightarrow{F}_{\nu m,q} \right) \tag{5.8}$$

where $\overline{\overline{\tau_q}}$ is the q^{th} phase stress-strain tensor :

$$\overline{\overline{\tau_q}} = \alpha_q \mu_q \left(\nabla \overrightarrow{\nu}_q + \nabla \overrightarrow{\nu}_q^T \right) + \alpha_q \left(\lambda_q - \frac{2}{3} \mu_q \right) \nabla \cdot \overrightarrow{\nu}_q \overline{\overline{I}} \tag{5.9}$$

Here μ_q and λ_q are the shear and the bulk viscosity of phase q , $\overrightarrow{F}_q$ is an external body force, $\overrightarrow{F}_{lift,q}$ is a lift force, $\overrightarrow{F}_{\nu m,q}$ is a virtual mass force, $\overrightarrow{R}_{pq}$ is an interaction force between phases, and p is the pressure shared by all phases.

$\overrightarrow{\nu}_{pq}$ is the interphase velocity, defined as follows. If $\dot{m}_{pq} > 0$ (i.e., phase p mass is being transferred to phase q), $\overrightarrow{\nu}_{pq} = \overrightarrow{\nu}_p$; if $\dot{m}_{pq} < 0$ (i.e., phase q mass is being transferred to phase p), $\overrightarrow{\nu}_{pq} = \overrightarrow{\nu}_q$. Likewise, if $\dot{m}_{qp} > 0$ then $\overrightarrow{\nu}_{qp} = \overrightarrow{\nu}_q$, if $\dot{m}_{qp} < 0$ then $\overrightarrow{\nu}_{qp} = \overrightarrow{\nu}_p$.

The $\overrightarrow{F}_{\nu m,q}$ virtual mass force is considered zero by default, as well as the lift force $\overrightarrow{F}_{lift,q}$, for reasons discussed in 5.8. The equation 5.8 must be closed with appropriate expressions for the interphase force $\overrightarrow{R}_{pq}$. The program uses a simple interaction term, in the following form :

$$\sum_{p=1}^{n} \overrightarrow{R}_{pq} = \sum_{p=1}^{n} K_{pq} (\overrightarrow{\nu}_p - \overrightarrow{\nu}_q) \tag{5.10}$$

where K_{pq} $(= K_{qp})$ is the interphase momentum exchange coefficient.

So, considering the above and $\dot{m}_{pq} = \dot{m}_{qp} = 0$, the general equations take the following form for the gas and solid phase :

Gas phase :

$$\frac{\partial}{\partial t}(\alpha_g \rho_g \overrightarrow{\nu}_g) + \nabla \cdot (\alpha_g \rho_g \overrightarrow{\nu}_g \overrightarrow{\nu}_g) = -\alpha_g \nabla p + \nabla \cdot \overline{\overline{\tau_g}} + \alpha_g \rho_g \overrightarrow{g} + \overrightarrow{K}_{sl} (\overrightarrow{\nu}_g - \overrightarrow{\nu}_s) \tag{5.11}$$

Solid phase :

$$\frac{\partial}{\partial t}(\alpha_s \rho_s \overrightarrow{\nu}_s) + \nabla \cdot (\alpha_s \rho_s \overrightarrow{\nu}_s \overrightarrow{\nu}_s) = -\alpha_s \nabla p + \nabla \cdot \overline{\overline{\tau}}_s + \alpha_s \rho_s \overrightarrow{s} + \overrightarrow{K}_{sl}(\overrightarrow{\nu}_g - \overrightarrow{\nu}_s) \tag{5.12}$$

where the solid-phase stress tensor is given by :

$$\overline{\overline{\tau}}_s = \alpha_s \mu_s \left(\nabla \overrightarrow{\nu}_s + \nabla \overrightarrow{\nu}_s^T\right) + \alpha_s \left(\lambda_s - \frac{2}{3}\mu_s\right) \nabla \cdot \overrightarrow{\nu}_s \overline{\overline{I}}_s \tag{5.13}$$

The various interphase exchange coefficients are described in 5.7.1.

5.6 Conservation of Energy

To describe the conservation of energy in Eulerian multiphase applications, a separate enthalpy equation is written for each phase:

$$\begin{aligned}\frac{\partial}{\partial t}(\alpha_q \rho_q h_q) + \nabla \cdot (\alpha_q \rho_q \overrightarrow{u_q} h_q) =& \alpha_q \frac{\partial p_q}{\partial t} + \overline{\overline{\tau}} : \nabla \overrightarrow{u_q} - \nabla \cdot \overrightarrow{q_q} \\ &+ S_q + \sum_{p=1}^{n} (Q_{pq} + \dot{m}_{pq} h_{pq} - \dot{m}_{qp} h_{qp})\end{aligned} \tag{5.14}$$

where h_q is the specific enthalpy of the q^{th} phase, $\overrightarrow{q_q}$ is the heat flux, S_q is a source term that includes sources of enthalpy (e.g., due to chemical reaction or radiation), Q_{pq} is the intensity of heat exchange between the p^{th} and q^{th} phases, and h_{pq} is the interphase enthalpy (e.g., the enthalpy of the vapor at the temperature of the droplets, in the case of evaporation). The heat exchange between phases must comply with the local balance conditions, $Q_{pq} = -Q_{qp}$ and $Q_{qq} = 0$.

5.7 Kinetic Theory of Granular Flow (KTGF)

5.7.1 Interphase exchange coefficients

Fluid-Solid exchange coefficient

The fluid-solid exchange coefficient K_{sl} can be written in the following general form :

$$K_{sl} = \frac{\alpha_s \rho_s f}{\tau_s} \tag{5.15}$$

Where f is defined differently for the different exchange-coefficient models, and τ_s, the 'particulate relaxation time', is defined as :

$$\tau_s = \frac{\rho_s d_s^2}{18\mu_l} \tag{5.16}$$

where d_s is the diameter of particles of phase s.

All definitions of f include a drag function (C_D) that is based on the relative Reynolds number (Re Re_s). It is this drag function that differs among the exchange-coefficient models. In this study, the Gidaspow model is used as it is recommended by Fluent for dense fluidized beds .

The D. Gidaspow (1992) model is a combination of the C.-Y. Wen (1966) model and the Ergun (1952) equation .

When $\alpha_l > 0.8$, the fluid-solid exchange coefficient K_{sl} is of the following form :

$$K_{sl} = \frac{3}{4} C_D \frac{\alpha_s \alpha_l \rho_l |\overrightarrow{\nu}_s - \overrightarrow{\nu}_l|}{d_s} a_l^{-2.65} \tag{5.17}$$

where

$$C_D = \frac{24}{\alpha_l Re_s}[1 + 0.15(\alpha_l Re_s)^{0.687}] \tag{5.18}$$

and

$$Re_s = \frac{d_s \rho_g |\overrightarrow{\nu}_s - \overrightarrow{\nu}_l|}{\mu_g} \tag{5.19}$$

When $\alpha_l \leq 0.8$,

$$K_{sl} = 150 \frac{\alpha_s (1 - \alpha_l)\mu_l}{\alpha_l d_s^2} + 1.75 \frac{\rho_l \alpha_s |\overrightarrow{\nu}_s - \overrightarrow{\nu}_l|}{d_s} \tag{5.20}$$

Solid-Solid exchange coefficient

The symmetric Syamlal (1987) model is recommended for a pair of solids, where the solid-solid exchange coefficient K_{ls} has the following form :

$$K_{ls} = \frac{3(1+e_{ls})(\frac{\pi}{2}+C_{fr,ls}\frac{\pi^2}{8})\alpha_s\rho_s\alpha_l\rho_l(d_l+d_s)^2 g_{0,ls}}{2\pi(\rho_l d_l^3+\rho_s d_s^3)}|\overrightarrow{\nu}_s - \overrightarrow{\nu}_l| \tag{5.21}$$

where

e_{ls} = the restitution coefficient
$C_{fr,ls}$ = the coefficient of friction between the l^{th} and s^{th} solid-phase particles ($C_{fr,ls} = 0$)
d_l = the diameter of the particles of solid l
$g_{0,ls}$ = the radial distribution coefficient (see 5.7.4)

5.7.2 Solids Pressure

For granular flows in the compressible regime (i.e., where the solids volume fraction is less than its maximum allowed value), a solids pressure is calculated independently and used for the pressure gradient term, ∇p_s, in the granular-phase momentum equation 5.8. Because a Maxwellian velocity distribution is used for the particles, a granular temperature is introduced into the model, and appears in the expression for the solids pressure and viscosities. The solids pressure is composed of a kinetic term and a second term due to particle collisions:

$$p_s = \alpha_s\rho_s\Theta_s + 2\rho_s(1+e_{ss})\alpha_s^2 g_{0,ss}\Theta_s \tag{5.22}$$

where e_{ss} is the coefficient of restitution for particle collisions, $g_{0,ss}$ is the radial distribution function, and Θ_s is the granular temperature. The granular temperature Θ_s described in 5.7.5, is proportional to the kinetic energy of fluctuating particle motion. The function $g_{0,ss}$ described in 5.7.4, is a distribution function that governs the transition from the compressible condition with $\alpha < \alpha_{s,max}$, where the spacing between the solids can continue to decrease, to the incompressible condition with $\alpha = \alpha_{s,max}$, where no further decrease in the spacing an occur. It is an important parameter in the description of the solids pressure, resulting from granular kinetic theory. The default value for the coefficient of restitution for particle collisions was used, $e_{ss} = 0.9$.

5.7.3 Solid shear stresses

The solids stress tensor contains shear and bulk viscosities arising from particle momentum exchange, due to translation and collision. A frictional component of viscosity is also included to

account for the viscous-plastic transition that occurs when particles of a solid phase reach the maximum solid volume fraction.

The collisional and kinetic parts, and the optional frictional part, are added to give the solids shear viscosity:

$$\mu_s = \mu_{s,col} + \mu_{s,kin} + \mu_{s,fr} \tag{5.23}$$

where the collision viscosity of the solids $\mu_{s,col}$ is modelled as, D. Gidaspow (1992); M. Syamlal (1993):

$$\mu_{s,col} = \frac{4}{5}\alpha_s \rho_s d_s g_{0,ss}(1+e_{ss})\sqrt{\frac{\Theta_s}{\pi}}\alpha_s \tag{5.24}$$

and the kinetic viscosity as an expression from D. Gidaspow (1992) :

$$\mu_{s,kin} = \frac{10\rho_s d_s \sqrt{\Theta_s \pi}}{96\alpha_s(1+e_{ss})g_{0,ss}}\left[1+\frac{4}{5}g_{0,ss}\alpha_s(1+e_{ss})\right]^2\alpha_s \tag{5.25}$$

The solids bulk viscosity accounts for the resistance of the granular particles to compression and expansion. The model of C. K. K. Lun (1984) was used :

$$\lambda_s = \frac{4}{5}\alpha_s \rho_s d_s g_{0,ss}(1+e_{ss})\sqrt{\frac{\Theta_s}{\pi}} \tag{5.26}$$

When a solid phase is near the packing limit, the generation of stress is mainly due to friction between particles. Ansys Fluent provides Schaeffer (1987) expression for frictional viscosity :

$$\mu_{s,fr} = \frac{p_s sin(\phi)}{2\sqrt{I_{2D}}} \tag{5.27}$$

where p_s is the solids pressure, ϕ is the angle of internal friction, and I_{2D} is the second invariant of the stress tensor. The frictional stress is added to the stress predicted by the kinetic theory when the solids volume fraction exceeds a critical value. This value is called friction packing limit $\alpha_{s,fr}$, and is set to 0.5 when the flow is three-dimensional and the maximum packing limit $\alpha_{s,max}$ is set to 0.63 as proposed by Ansys Fluent.

The solids pressure p_s , Eq. 5.22, represents the normal force due to particle interactions, and the angle of internal friction is given by :

$$\phi = -3K_{sl}\Theta_s \tag{5.28}$$

5.7.4 Radial Distribution

The radial distribution function g_0, is a correction factor that modifies the probability of collisions between grains when the solid granular phase becomes dense. In the literature there is no unique formulation for the radial distribution function. The model of D. Ma (1990) for n solid phases was used :

$$g_{0,ll} = \frac{1 + 2.5\alpha_s + 4.59\alpha_s^2 + 4.52\alpha_s^3}{\left(1 - \left(\frac{\alpha_s}{\alpha_{s,max}}\right)^3\right)^{0.678}} + \frac{1}{2} d_l \sum_{k=1}^{N} \frac{\alpha_k}{d_k} \tag{5.29}$$

5.7.5 Granular Temperature

The granular temperature for the s^{th} solids phase is proportional to the kinetic energy of the random motion of the particles. The transport equation derived from kinetic theory has the form, J. Ding (1990) :

$$\frac{3}{2}\left[\frac{\partial}{\partial t}\left(\rho_s \alpha_s \Theta_s\right) + \nabla \cdot \left(\rho_s \alpha_s \overrightarrow{\nu_s} \Theta_s\right)\right] = \left(-p_s \overline{\overline{I}} + \overline{\overline{\tau_s}}\right) : \nabla \overrightarrow{\nu_s} + \nabla \cdot \left(k_{\Theta_s} \nabla \Theta_s\right) - \gamma_{\Theta_s} + \phi_{ls} \tag{5.30}$$

where

$(-p_s \overline{\overline{I}} + \overline{\overline{\tau_s}}) : \nabla \overrightarrow{\nu_s}$ = the generation of energy by the solid stress tensor

$k_{\Theta_s} \nabla \Theta_s$ = the diffusion of energy (k_{Θ_s} is the diffusion coefficient)

γ_{Θ_s} = the collisional dissipation of energy

ϕ_{ls} = the energy exchange between the l^{th} solid or fluid phase and the s^{th} solid phase

The diffusion coefficient is given by the model of D. Gidaspow (1992) :

$$k_{\Theta_s} = \frac{150\rho_s d_s \sqrt{(\Theta\pi)}}{384(1 + e_{ss}) g_{0,ss}} \left[1 + \frac{6}{5}\alpha_s g_{0,ss}(1 + e_{ss})\right]^2 + 2\rho_s \alpha_s^2 d_s (1 + e_{ss}) g_{0,ss} \sqrt{\frac{\Theta_s}{\pi}} \tag{5.31}$$

and the collisional dissipation energy is given by C. K. K. Lun (1984):

$$\gamma_{\Theta_s} = \frac{12(1-e_{ss}^2)g_{0,ss}}{d_s\sqrt{\pi}}\rho_s\alpha_s^2\Theta_s^{3/2} \tag{5.32}$$

Here, the algebraic formulation for the granular temperature was chosen, which is obtained by neglecting convection and diffusion in the transport equation, Eq. 5.30, M. Syamlal (1993).

5.8 Lift Forces

For multiphase flows, the effect of lift forces on the secondary phase particles (or droplets or bubbles) can be included. These lift forces act on a particle mainly due to velocity gradients in the primary-phase flow field. The lift force will be more significant for larger particles so their inclusion is not appropriate for closely packed or very small particles, as proposed by Ansys Fluent. Furthermore, the existing lift forces are insignificant, compared to drag forces.

5.9 Viscous Model

Viscosity is a measure of the resistance of a fluid when deformed by either shear stress or tensile stress. It describes the fluid's internal resistance to flow and may be thought of as a measure of fluid friction. In some applications the fluids used are considered as ideal or inviscid, but since all real fluids (except superfluids) are viscous, we apply a viscous model in this study.

Turbulence is the three-dimensional unsteady random motion observed in fluids at moderate to high Reynolds numbers. Almost all technical flows are turbulent and interesting quantities such as mixing of momentum, energy and species, heat transfer, pressure losses and forces on aerodynamic bodies, are dependent on turbulence. While it is described by Navier-Stokes equations, it is not feasible to resolve the wide range of scales in time and space using Direct Numerical Simulation (DNS), due to limited computing power. This is why averaging procedures are applied to the Navier-Stokes equations, to filter out parts of the turbulent spectrum.

Using Reynolds-averaging (time-averaging) procedures the result is Reynolds-Averaged Navier-Stokes equations (RANS), which eliminates all turbulent structures from the flow and a smooth variation of the averaged velocity, and pressure fields can be obtained. This process introduces additional unknown terms into the transport equations (Reynolds Stresses and Fluxes), which have to be provided by suitable turbulence models. The model choice, as far as the numerical grid, are crucial for the quality of simulation.

Using Scale-Resolving Simulation (SRS) methods, a part of the turbulence spectrum is resolved in at least one part of the flow domain. Such method is the Large Eddy Simulation (LES), but hybrids are appearing (RANS and LES). SRS methods require time-resolved simulations with small time steps, making them computationally more expensive than RANS simulations. The choice of the model has to be made considering the physics of the flow, the level of accuracy required, the available computational resources and the amount of available time for the simulation.

The $k-\varepsilon$ models solve two transport equations and model the Reynolds Stresses using the Eddy Viscosity approach. The standard $k-\varepsilon$ model has generally been used for flow calculations since it was proposed by B. E. Launder (1974). It is applied for industrial flow and heat transfer simulations, due to robustness, economy and reasonable accuracy. In this study, the Realizable $k-\varepsilon$ turbulence model is applied, B. E. Launder (1974), as proposed by Ansys Fluent comparatively to the other $k-\varepsilon$ models.

5.10 Radiation Model

The radiation model used in this study is P-1, considering only gray radiation. This means that the gas phase is transparent, and no other than gray radiation is modelled.

5.11 Modelling species transport

Modelling species mixing and transport is achieved by solving conservation equations describing convection, diffusion, and reactions sources for each specie. Ansys Fluent predicts the local mass fraction for each specie, Y_i , through the solution of a convection-diffusion equation, for the i^{th} species. This equation has the general form :

$$\frac{\partial}{\partial t}(\rho Y_i) + \nabla \cdot (\rho \overrightarrow{\nu} Y_i) = -\nabla \cdot \overrightarrow{J}_i + R_i + Si \tag{5.33}$$

where R_i is the net rate of production of species i by chemical reaction, and S_i is the rate of creation by addition from the dispersed phase. An equation of this form will be solved for N-1 species, where N is the total number of fluid phase chemical species, present in the system. The N^{th} mass fraction is determined as one minus the sum of the N-1 solved mass fractions, since the total mass fraction must sum to unity.

Chapter 6

Model description

A three-dimensional computational model was developed to describe the biomass gasification process inside a steam fluidized bed reactor. The commercial multi-purpose CFD code FLUENT 13.0 was used, taking into account drying, devolatilization, combustion and gasification processes. Three phases were used to model the reactor (sand, solid phase for the fuel, and gas phase). Sand and solid phase were described using the kinetic theory of granular flows. All phases were described using an Eulerian approach to model the exchange of mass, energy and momentum. The chemical model consists of three (3) heterogeneous and two (2) homogeneous reactions. Drying and devolatilization were supposed instantaneous at the biomass feed region. All reaction-rates were determined by Arrhenius equations, the kinetic parameters of which were found in literature. The gasifier was operated and studied at atmospheric condition. Validation was performed, by comparing the model with experimental results.

6.1 Euler-Euler approach

The Euler-Euler approach was chosen for the simulation of the gasifier. This is because, with current and expected future computer resources, it does not seem feasible to use more detailed models, such as Euler-Lagrange methods, that can lead to industrial scale reactors.

In the Euler-Euler modelling approach, the particulate phase is considered as a continuous phase interpenetrating and interacting with the gas phase. Polydisperse systems can be modelled within this approach via multiple solid phases, where each phase characterizes a different particle class. The kinetic theory of granular flow is used as a theoretical framework, to derive constitutive equations for the solid phases and the gas-particle interactions. However, the Euler-Euler model has to be accompanied with closure models describing the mass, momentum and energy transfer between multiple continuous phases ,Fluent.

In order to succeed convergence within acceptable computational time, some simplifying assumptions were incorporated to the models of fluid dynamics and chemical reactions, involved in biomass gasification, as follows :

- The solid particles inside the bed are spherical, with constant diameters
- The kinetic theory of granular flow (KTGF) is used in the transport equation, to describe the particle collision and fluctuation in the gasifier
- Drying and devolatilization are considered to occur instantaneously, at the feed region, Liang Yu (2007)
- The gas phase is assumed transparent, so that radiative energy is neither absorbed nor emitted, Liang Yu (2007). The main heat transfer mechanism is convection
- The carbon hydrogenation $C + H_2 \rightarrow CH_4$, and the methanation reaction $CO + 3H_2 \rightarrow CH_4 + H_2O$, were not considered because they both require high pressure and catalysts.

6.2 Biomass fuel

The fuel used in this study is Agrol softwood pellets [1]. They are made from the sawdust and shavings created by lumber mills. A single lumber mill may be the only source of raw material needed for a pellet mill, and much of the lumber is softwood. The trees are de-barked before cut into lumber, so there is very little dirt or bark in the sawdust, creating a very light colored, clean, low ash pellet, as shown in Figure 6.1, with consistent burning characteristics.

Figure 6.1: Biomass -Agrol softwood pellets

No additives are used to make the pellets, as natural lignin of the wood acts as a binder. There are also pellets made from agricultural waste products and prairie grasses. These pellets have slightly higher ash content, but provide a larger source of raw materials. Some of the raw material may be sawdust, wood chips, lumber mill scrap, and even full trees unsuitable for lumber. The raw materials may be green, or freshly cut, may be partial dry, or even kiln dried. By processing these raw materials all in the same way, the end product has consistent moisture content, heat value, ash content, and burn characteristics, Woodpellets. The proximate and ultimate analysis

[1] Agrol Wood Pellets conform to Swedish SS 187120 standard and German DIN+ standard for Domestic Grade 1 pellets and are of premium quality.

of the Agrol softwood pellets, used in this study, is given in Table 6.1.

Softwood pellets are presently used in small-scale residential combustion units, and the market will further increase within the next years. Pellets may also be used in small-scale, fixed-bed gasifiers for heating purposes as well as regarding micro-CHP applications (e.g. Stirling engine or micro-turbine).

Table 6.1: Proximate and ultimate analysis of Agrol wood-pellets

Proximate analysis		**Ultimate analysis (%w/w dry basis)**	
Volatiles (%w/w dry)	81.5	C	47.4
Fixed carbon (%w/w dry)	13.6	H	6.4
Moisture (%w/w)	4.8	O	46.0
Ash	0.1	N	0.1
Heating Value		S	0.1
LHV (kJ/kg wet)	20.600		

6.3 Reactor's geometry

The modelled gasifier is a laboratory scale, allothermal bubbling fluidized bed reactor, owned by the Technical University of Munich. It has cylindrical shape with an internal concentric cylinder for the biomass inlet. The steam is inserted through holes at the bottom of the reactor in cross formation. The feed point of biomass is near the steam inlet, so that the biomass pellets get scattered by the nearby steam stream. The whole geometry is axisymmetric. The required heat for the endothermic gasification reactions is provided by electrically heated heatpipes. The gasifier is illustrated in Fig. 6.2.

The main design data are presented in Table 6.2. The experimental facility consists of the following parts :

1. Pressure vessel gasifier
2. High temperature heatpipes
3. Electrical heating
4. Screwing feeding system and lock hopper system
5. Cyclone
6. High temperature ceramic candle filter

Biomass is fed through a screwing feeding system directly inside the bubbling fluidized bed reactor. The maximum fuel input is 50 kW_{th}, based on woody biomass. The cylindrical vessel

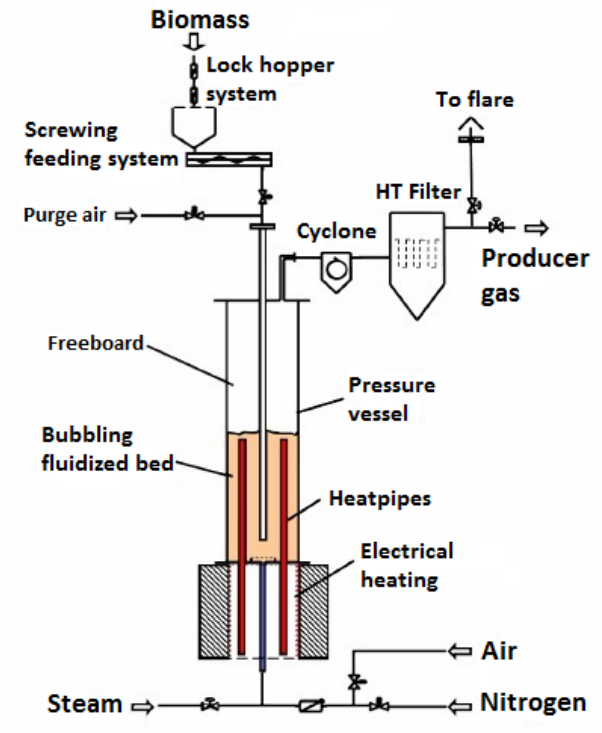

Figure 6.2: TUM gasification test rig

Table 6.2: Main dimensions of the gasifier

Part	**Feature**	**Value**	**Units**
Reactor vessel	Reactor length	1500	mm
	Reactor diameter (internal)	154	mm
	Fluidized bed height	700	mm
	Freeboard height	800	mm
Fuel injection tube	Tube diameter	48	mm
	Tube height inside the vessel	1400	mm
	Position of the tube in the reactor	center	-
Heatpipes (x4)	Heatpipe diameter	19	mm
	Heatpipe length inside the reactor	650	mm
Steam injection holes	Diameter	1.5	mm
Output of the producer gas	Hole diameter	21	mm
Bed material (olivine sand)	Bulk density	1450	kg/m^3
	Average diameter of the particles	200	μm
Wood pellets	Length of the pellet	20	mm
	Diameter of the pellet	6	mm
	Average density of pellets	1.2	g/cm^3

is made of stainless steel (AISI314, DIN X15 CrNiSi 25 20, 1.4841), which can be pressurized up to 5 bar. The screwing feeding system is a rectangular vessel ($20l$ volume) with a screwer, which can be pressurized as well (up to 10 bar). A lock hopper system is coupled to the screwing feeding system, to secure the continuous filling of the rectangular vessel with biomass pellets.

The bed is fluidized with steam and olivine is the bed material. Oversaturated steam is produced by a steam generator and after being heated to a temperature of 530 $°C$ with the help of a superheater, is injected into the reactor through an injection cross. Pressure loss is measured by differential pressure sensors placed at the bottom and top of the reactor vessel respectively. Bed and freeboard temperature are controlled by type K thermocouples located all over the entire length of the gasifier.

The producer gas exits the reactor at the top and after its way through a cyclone, it is driven to a high temperature ceramic candle filter, for further purification. The remaining unreacted char particles are separated and removed at the cyclone.

6.4 Computational grid

The reactor was modelled using a 3D computational grid. The geometry, as described in the last section, was built using the program Gambit. In total 865.000 hexahedral cells were used, and a part of the bottom grid is shown below :

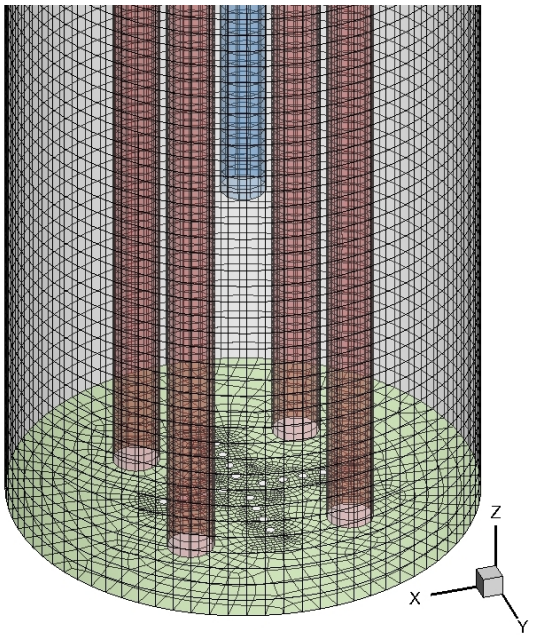

Figure 6.3: Computational mesh

Here, the steam inlet holes in the cross formation can be identified at the green bottom of the reactor. The four heatpipes are shown in red, and the fuel injection tube in blue. Biomass is fed

through the base of the blue tube, which is hollow. The producer gas exits the geometry at the upper part through a hole. All surfaces, except holes, are considered impermeable walls.

6.5 Biomass Heatpipe Reformer-BioHPR (TUM)

The Biomass Heatpipe Reformer (BioHPR) is an innovative gasification concept for allothermal heat transfer, through high temperature heatpipes.

The heatpipes are heat exchangers, based on enclosed two-phase systems. The components are a hermetic sealed container, a wick structure and a small amount of working fluid (usually acetone, ethanol, water, sodium, mercury, etc.,) which is in equilibrium with its own vapour. The heatpipe is divided in three zones : the evaporation zone, where heat is provided to the heatpipe, the condensation zone, where heat is provided to the environment and the middle section, which is called adiabatic zone. The operational principle of the heatpipe is illustrated in Fig. 6.4.

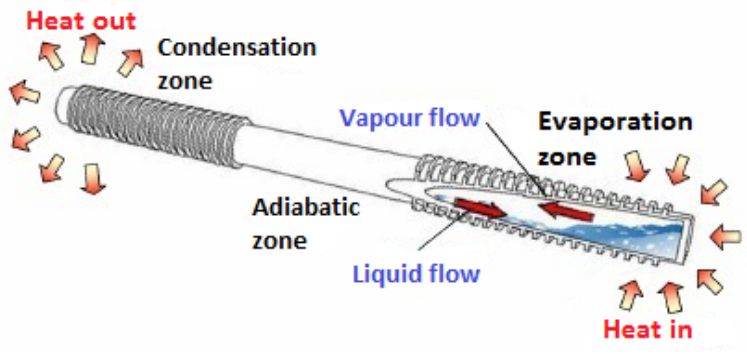

Figure 6.4: Operational principle of a heatpipe.

Heatpipes utilise the phase change of a working fluid operating in a completely evacuated and sealed enclosure. The fluid exists within the pipe as a wet saturated vapour. When heat is applied to the evaporation zone, the working fluid is evaporated and then condenses at the condensation zone, by giving the applied heat back to its environment. This process is continuously ongoing as long as there is a sufficient capillary pressure, to drive the condensate back to the evaporation zone. The latent heat of vaporization during the phase change process is utilized, resulting in a very efficient energy transfer.

In bigger facilities, a combustion chamber could be used below the gasifier for the heat transfer at the evaporation zone, by burning the remaining char particles from the cyclone. Furthermore, with this formation the lower part of the gasifier is heated through radiation from the combustion chamber. Regarding this study, the heatpipes are electrically heated. In the simulation models, the heatpipes are modelled as impermeable wall surfaces with no slip condition for shear stresses, and have a constant temperature of 1100 $^{\circ}C$ at their outer surface.

6.6 Phases and Materials

The case was simulated using three (3) phases, which enter the gasifier through boundary conditions, and interact exchanging mass, momentum, temperature and species. Those three (3) phases are :

1. Gas phase - Primary. The gas phase is used for simulating both the steam inlet and the product gas outlet. This is achieved by including all the working species in one phase, so that the mass and momentum equations are solved once per time step. It consists of O_2, N_2, H_2O, H_2, CO, CO_2 and CH_4. The properties of the aforementioned species where taken from Ansys Fluent database.
   The gasifying agent is steam, as discussed in 3.2, with a constant mass flow rate.

2. Sand - Secondary phase. This phase represents the fluidizing bed material, which is olivine in our study. The sand is modelled granular and inert, with a constant diameter of 200 μm and density 1450 kg/m^3, belonging to Geldart B group. The remaining properties of sand were taken from Ansys Fluent database.

3. Solid - Secondary phase. This phase simulates the fuel inlet of the gasifier. It is considered to be a granular phase, with a constant diameter of 6 mm. It consists of solid carbon C_s representing char, H_2O for the fuel's moisture, CH_4 for the volatile matter, and ash. The granular properties of sand and solid phase are the same, and summarized in Table 6.3.

Table 6.3: Properties of granular phases

Properties	**Model**	**Equation**
Granular viscosity $\mu_{s,kin}$, $(kg/m \cdot s)$	D. Gidaspow (1992)	5.25
Granular bulk viscosity λ_s, $(kg/m \cdot s)$	C. K. K. Lun (1984)	5.26
Frictional viscosity $\mu_{s,fr}$, $(kg/m \cdot s)$	Schaeffer (1987)	5.27
Angle of internal friction $\phi = 30$ deg	default, Fluent	5.28
Frictional pressure ∇p_{fr}, (N/m^2)	KTGF, J. Ding (1990)	-
Frictional modulus (N/m^2)	Derived, Fluent	-
Friction packing limit $\alpha_{s,fr}$, $(-)$	constant=0.5	-
Granular temperature Θ, (m^2/s^2)	M. Syamlal (1993)	5.30
Solids pressure ∇p_s, (N/m^2)	C. K. K. Lun (1984)	5.22
Radial distribution g_0, $(-)$	D. Ma (1990)	5.29
Elasticity modulus (N/m^2)	Derived, Fluent	-
Packing limit $\alpha_{s,max}$, $(-)$	constant=0.62	-

6.6.1 Boundary Conditions

The base of the internal cylinder is the particle inlet, from which the wood pellets enter the reactor, while the steam is inserted through the bottom of the reactor. Along with the wood pellets, purge air is simulated to insert through the particle inlet surface. This amount of air is constant 2 lt/min. The boundary conditions of the case remain constant, and are demonstrated in Tables 6.4 and 6.5. The species mass fractions occur from the proximate analysis of the wood-pellets (Table 6.1) :

Table 6.4: Main boundary conditions

Experimental data	**Case Study**
Biomass mass flow	2 kg/h
Steam mass flow	2 kg/h
Pressure	1 atm

Table 6.5: Specific boundary conditions

Boundary conditions	**Solid Phase**	**Gas Phase**	
Zone name	Particle Inlet	Particle Inlet	Steam Inlet
Turbulence intensity (%)	10	10	10
Hydraulic diameter (m)	0.01	0.01	0.004
Total temperature (K)	300	300	800
Species mass fractions	Biomass	Air	Steam
H_2O	0.048	-	1
$C(s)$	0.136	-	-
CH_4	0.815	-	-
Ash	0.001	-	-
O_2	-	0.23	-
N_2	-	0.77	-

The STBR (steam to biomass ratio) can be found by applying Eq. 3.1, where the fuel moisture is $H_2O_{fuel} \cdot \dot{m}_{fuel}$:

$$STBR_1 = \frac{2kg/h + 0.048 \cdot 2kg/h}{(1 - 0.048) \cdot 2kg/h} = STBR_2 = \frac{5.2kg/h + 0.048 \cdot 5.2kg/h}{(1 - 0.048) \cdot 5.2kg/h} = 1.1 > 0.4 \quad (6.1)$$

6.7 System kinetics

The model's accuracy strongly depends on the chemical reactions chosen, and the reaction rates, which determine the final product gas composition. Sometimes in literature dependent reactions are taken into account, causing an unnecessary number of reactions, adding complexity and computational time. For this reason three (3) heterogeneous and two (2) homogeneous independent reactions were modelled. The main effects of the gas phase conversion process and the solid phase gasification are given by the following reactions. Rate constants are given in the form of the Arrhenius equation:

$$k = A \cdot exp(-E_\alpha / RT) \tag{6.2}$$

In this equation, A is the pre-exponential factor, and determines the speed of reaction, while E_α is the activation energy. R is the ideal gas constant ($R = 8.314 kJ/kgK$).

As already seen in sections 4.3, and 6.6, the total chemical reactions taking place inside the gasifier consist of drying, pyrolysis, homogeneous reactions in the gas phase and heterogeneous reactions between the gas and solid phase. All reactions are presented here :

1. Drying : $H_2O_{(s)} \rightarrow H_2O_{(g)}$ +40.7 MJ/Kmol
2. Pyrolysis : $Volatile_{(s)} = CH_{4(s)} \rightarrow CH_{4(g)}$ (no heat)
3. Partial oxidation of char : $C + \frac{1}{2}O_2 \rightarrow CO$ -111 MJ/Kmol
4. Boudouard reaction : $C + CO_2 \rightarrow 2CO$ +172 MJ/Kmol
5. Heterogeneous Water-gas reaction : $C + H_2O \rightarrow CO + H_2$ +131 MJ/Kmol
6. Water-gas shift reaction : $CO + H_2O \leftrightarrows CO_2 + H_2$ -41 MJ/kmol
7. Steam methane reforming reaction : $CH_4 + H_2O \leftrightarrows CO + 3H_2$ +206 MJ/kmol

The reaction rates, namely the pre-exponential factor and the activation energy were found in literature, cited in Table 6.6 :

Table 6.6: Kinetic rate parameters of simulated reactions

No.	Name	Reaction	A($1/s$)	$E_\alpha(kJ/mol)$	Reference
1	Char oxidation	$C + \frac{1}{2}O_2 \rightarrow CO$	11.12	130	Fennell PS (2005)
2	Boudouard	$C + CO_2 \rightarrow 2CO$	36.16	77.39	Y. Wang (1993)
3	Het. Water-gas	$C + H_2O \rightarrow CO + H_2$	15170	121.62	Y. Wang (1993)
4	Water-gas shift for.	$CO + H_2O \rightarrow CO_2 + H_2$	$2.98 * 10^{10}$	169	Coal gas.
5	Water-gas shift back.	$CO_2 + H_2 \rightarrow CO + H_2O$	$3 * 10^9$	130	Coal gas.
6	Steam reforming	$CH_4 + H_2O \rightarrow CO + 3H_2$	$2.98 * 10^{11}$	369	Coal gas.
7	CO oxidation	$CO + \frac{1}{2}O_2 \rightarrow CO_2$	$4.4 * 10^{12}$	168	Coal gas.

Chapter 7

Modelling approaches - Results

The results of the simulation models are presented here by means of charts. Comparison with the experimental data follows, for each approach.

7.1 Methane pyrolysis model - 1^{st} Approach

The first approach considers methane as the unique pyrolysis product. This means that the volatile matter of the fuel is transferred to the gas phase as methane. Figure 7.1, shows the volume of fraction (vof) of sand on discrete time steps from the beginning of the simulation until the steady state. It is plotted on the z-x plane of the reactor, for better visualization and comparison. The blue region is the freeboard, which has zero sand concentration while the coloured part non-zero, as explained at the legend on the side.

The maximum sand packing limit was set 0.62, so the red regions show packed conditions. This happens at the bottom of the reactor mostly around the steam stream, due to the weight of the sand column. The initial sand column was patched at 1 m, with a packing limit of 0.4 for the entire phase. This value was chosen so that the steam can easily penetrate through the sand phase from the beginning of the simulation process, away from packing conditions.

The actual 3d sand vof is shown through iso-surfaces at steady state, in figure 7.2. The fluidization and bubbling character of the bed is in good agreement with reality, but as it can be clearly observed, the total height of the sand is below the maximum height of the heatpipes, leading to a loss of energy transfer. The actual height of the sand should be slightly above the heatpipes level.

Problems encountered The sand level falls under the heatpipes mainly because of the initial selection of the sand height. Another reason is the compression of the sand column from the formation of a problematic solid-phase layer. As seen at 6.6, the solid phase consists of solid carbon C_s representing char, H_2O for the fuel's moisture, CH_4 for the volatile matter and ash. While C_s, H_2O and CH_4 react, they get released to the gas phase, leaving ash to be the only remaining specie inside the constant-diameter granular solid phase. As time passes, a layer of ash is inevitably formed on top of the sand column, like oil on water, as it can be seen in light blue color, at Fig. 7.3.

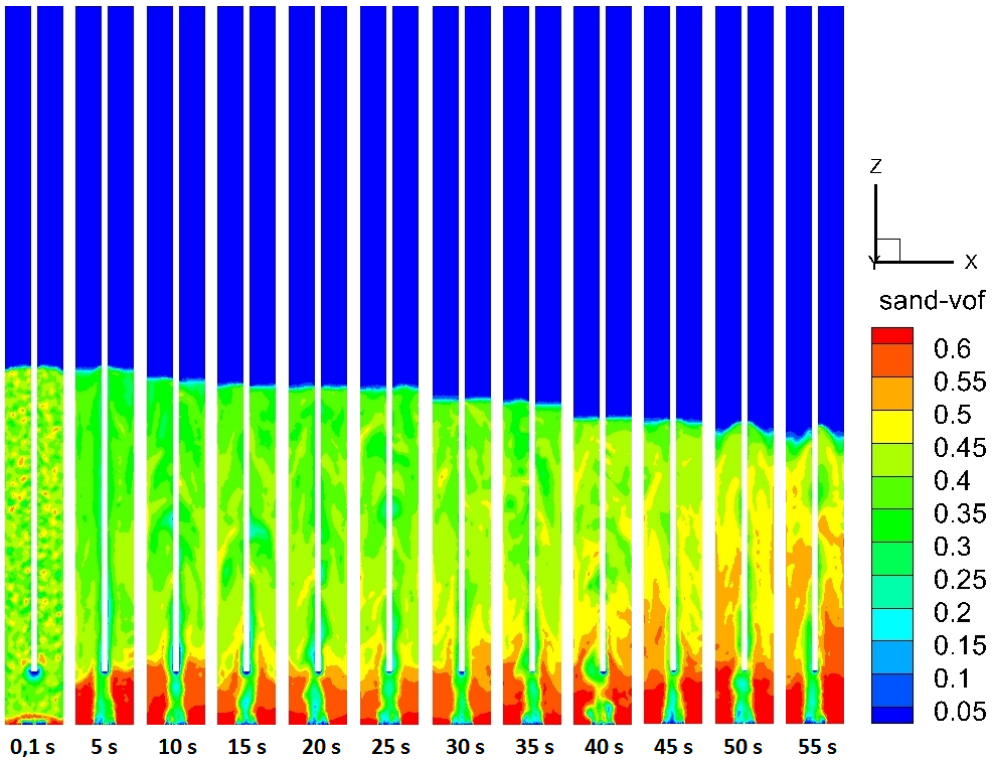

Figure 7.1: Sand volume of fraction

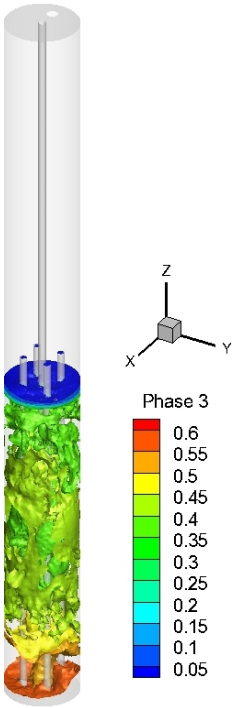

Figure 7.2: Sand volume of fraction 3d

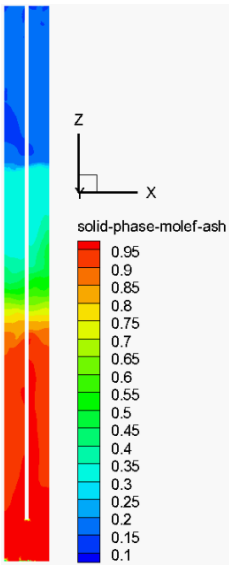

Figure 7.3: Ash layer above sand column

At Fig. 7.4, the operating conditions inside the reactor are presented at steady state. The static pressure and gas temperature are plotted on a straight line, starting from the bottom of the reactor, going all the way through the interior, and resulting at the center of the hole of the producer gas outlet.

As it can be seen, the static pressure shows a very good agreement with reality, falling linearly from the start until the end of the sand phase. Temperature has a constant value of 1150 K (877 $°C$) inside the sand phase, fluctuates around 1130 K inside the solid phase layer, and finally drops, as expected, at the freeboard region, having a constant value of 950 K (677 $°C$). This temperature drop happens very high inside the reactor because of the aforementioned problematic solid-phase layer.

At Fig. 7.5, the reaction rates of three (3) reactions at steady state are plotted on the same straight line used for presenting the results. As we can see, Boudouard and Het. Water-gas follow the exact same trend inside the sand column and become zero after exiting it. This is because they both refer to char, which is present only inside the sand phase. They both peak around 0.2 m, where the fuel is introduced to the reactor, and a second peak is right over the sand level indicating some char accumulation.

The methane reforming reaction takes place both inside the sand phase and the ash layer. It strongly peaks at the beginning of the freeboard at 1.45 m and results to zero around 1.8 m. All the reaction rates result to zero values, ensuring the equilibrium of the steady state condition.

At Fig. 7.6, the gas species are plotted at steady state throughout the reactor. The peak of H_2O at 0.2 m shows the high steam inlet at the bottom of the reactor. The mole fractions vary throughout the vertical axis because of the chemical reactions impact. Once again, the stable mole fractions at the outlet region ensure that steady state is reached.

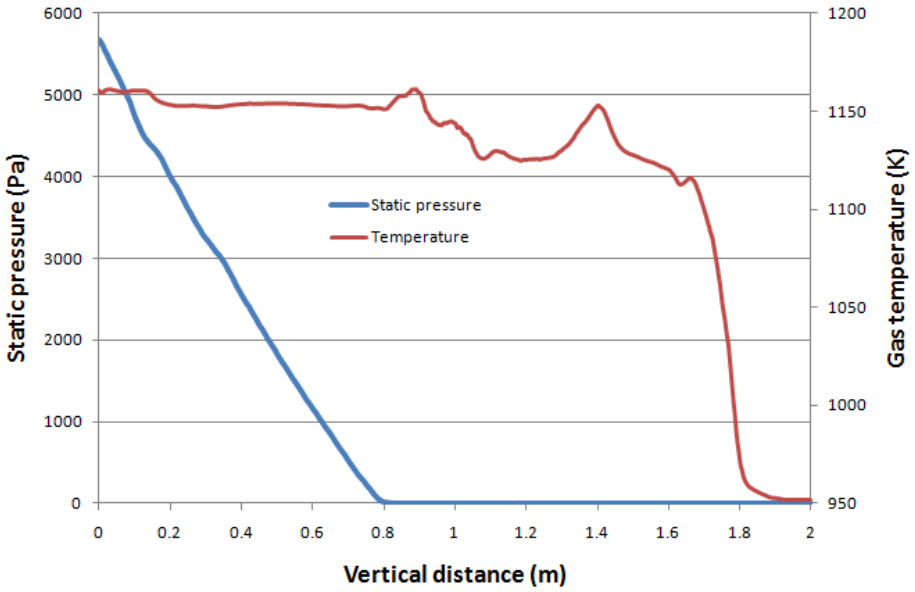

Figure 7.4: Operating conditions of gasifier at t=55 s

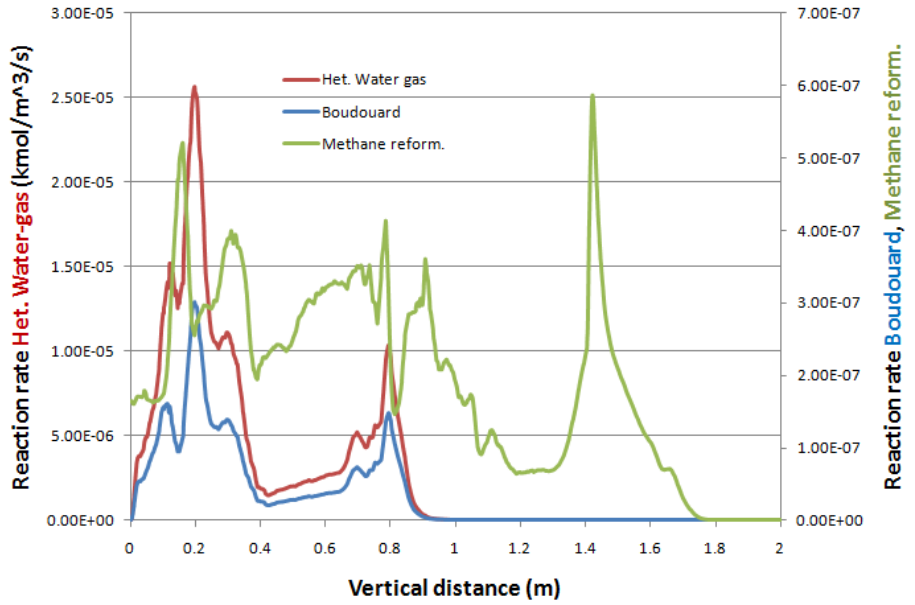

Figure 7.5: Reactions rates at t=55 s

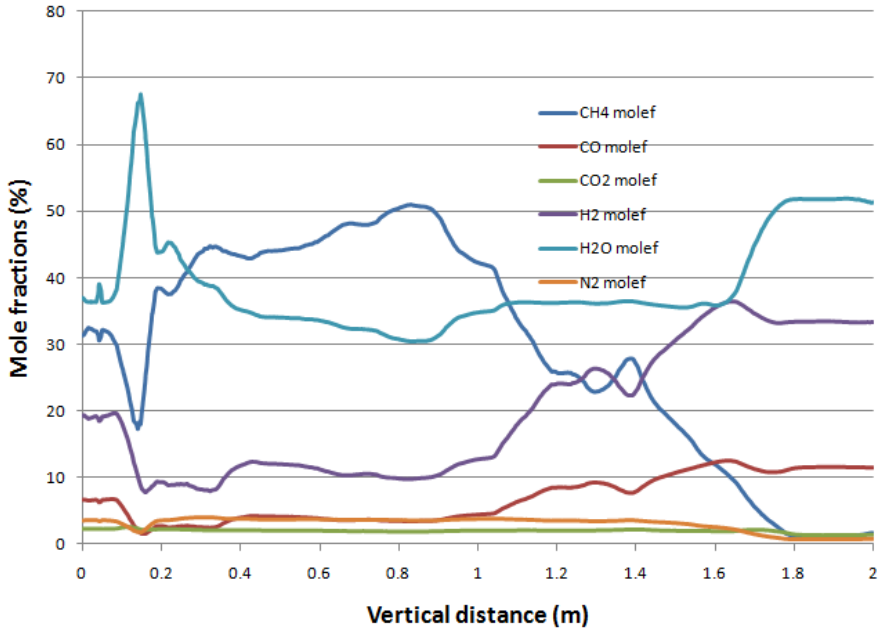

Figure 7.6: Mole fractions at t=55 s

Finally, the simulation results (as received (a.r.)) are compared to the actual experimental at Fig. 7.7. It is noticeable that H_2 and H_2O are overestimated, while CO_2 is underestimated. The CO, CH_4, and N_2 mole fractions show acceptable agreement with the experimental data. The reasons for these deviations can be grouped as follows :

1. The pyrolysis products were supposed to be 100% methane. This is an introductory assumption, but it is responsible for the model's accuracy. The gas synthesis is strongly related to the volatile matter and how this is modelled.

2. The reactions were supposed to be in equilibrium and the kinetic parameters were taken from literature.

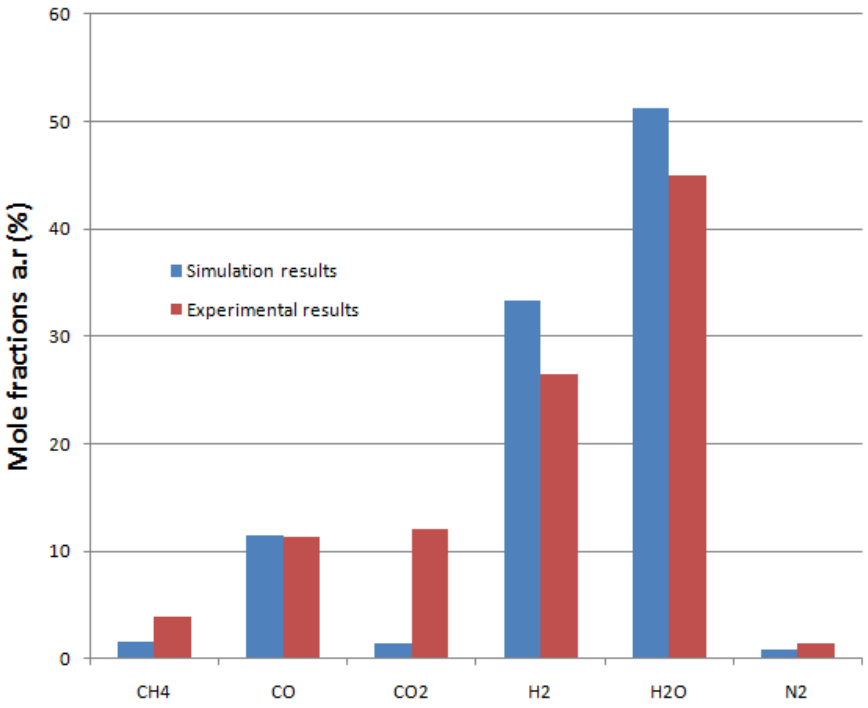

Figure 7.7: Outlet results

7.2 Seebauer model - 2^{nd} Approach

The Methane pyrolysis model was found to deviate from reality because of the many simplifying assumptions taken into account. This is why, further investigation had to be made on the topic.

In order to overcome the problematic solid-phase layer, a different modelling approach was considered. Again three (3) phases were introduced inside the gasifier. This time, ash was not modelled at all (the fuel has very low ash concentration and can be easily omitted with no significant error) and the solid phase consists only of C_s and N_2. By default, in Ansys Fluent, every phase has to contain an inert specie (N_2) for continuity reasons. When C_s reacts forming gaseous species, N_2 mass fraction increases inside the solid phase. This way, the solid-phase exists throughout the simulation process. The rest solid compounds were now supposed to be part of the gas phase, namely the fuel's moisture H_2O, and the volatile matter.

In order to move on with better simulation techniques, the volatile matter was now taken from the work of Seebauer (1999). The wood volatile consists of the species and proportions shown in Table 7.1.

This time, the sand was initially patched higher at 1.2 m, with the same packing limit of 0.4 to help the gas phase penetration through the sand phase. The maximum sand packing limit was again set to 0.62. As we can see in Fig. 7.8, the sand volume of fraction shows a better overall behaviour than before. No solid layer was created above the sand column, compressing it or limiting the freeboard.

Table 7.1: Composition of wood gas from the primary pyrolysis step according to Seebauer (1999)

Component	Mass fraction
H_2	0.032
CO	0.270
CO_2	0.386
CH_4	0.056
H_2O	0.256
Total	1.000

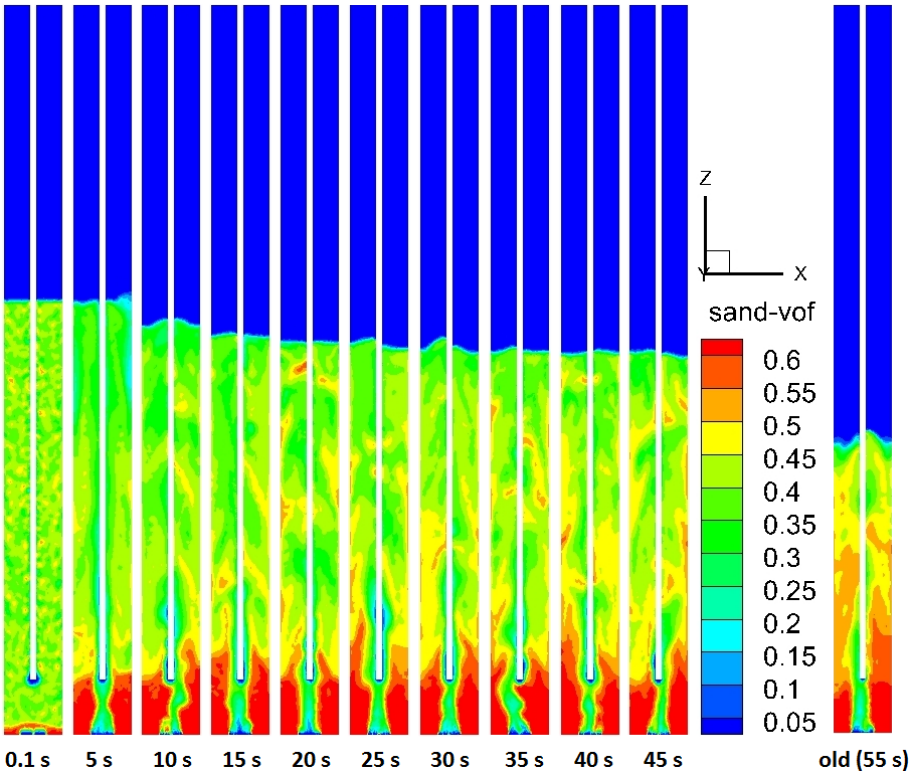

Figure 7.8: Sand volume of fraction

The bubbling character was achieved and steady state was reached at t=45 s. Further on, in Fig. 7.9, the sand level is above the heatpipes, covering them, as in reality.

At Fig. 7.10, the operating conditions inside the reactor are presented at steady state. The absolute pressure and gas temperature, on the same straight line inside the gasifier, are plotted.

The absolute pressure shows a very good and linear agreement with reality. It reaches the value of 1 bar at the exit of the sand column. Temperature has a constant value of 1090 K (817 $^{\circ}C$) inside the sand phase, and drops, as expected, at the freeboard region having a constant

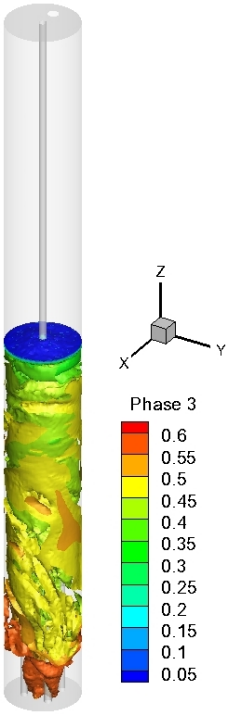

Figure 7.9: Sand volume of fraction 3d

value of 1050 K (777 $°C$) at the outlet. Now, the temperature drop happens right after the sand phase at 1.05 m, indicating the freeboard start.

At Fig. 7.11, three (3) reaction rates are shown. Now, the forward minus the backward CO shift, Boudouard and Heterogeneous reaction rates are plotted. The heterogeneous water gas refers to the char reaction with water. It peaks right after the fuel input at 0.4 m, and once again at the end of the sand level. At the freeboard, where no char is left to react, the reaction rate is zero. The same goes for Boudouard reaction, only to have much smaller reaction rates in general. The CO shift reaction (forward - backward,) shows that the forward rate is favoured inside the bed, while the backward at the freeboard. This is why we see some negative values after 1.1 m.

At Fig. 7.12, we see the mole fractions of the gas species at steady state plotted throughout the reactor. A better and more stable behaviour can be identified, showing better performance for this modelling approach.

Finally, the two simulation approaches (as received (a.r.)) are compared to the actual experimental at Fig. 7.13. With this second approach, H_2 and H_2O are fitted to the experimental data, but still CO is overestimated and CO_2 underestimated. Although the results show better agreement than those of the methane pyrolysis model, we still have some deviations from reality. Again some reasons for this are :

1. The pyrolysis products were taken from literature. The actual fuel pyrolysis products have

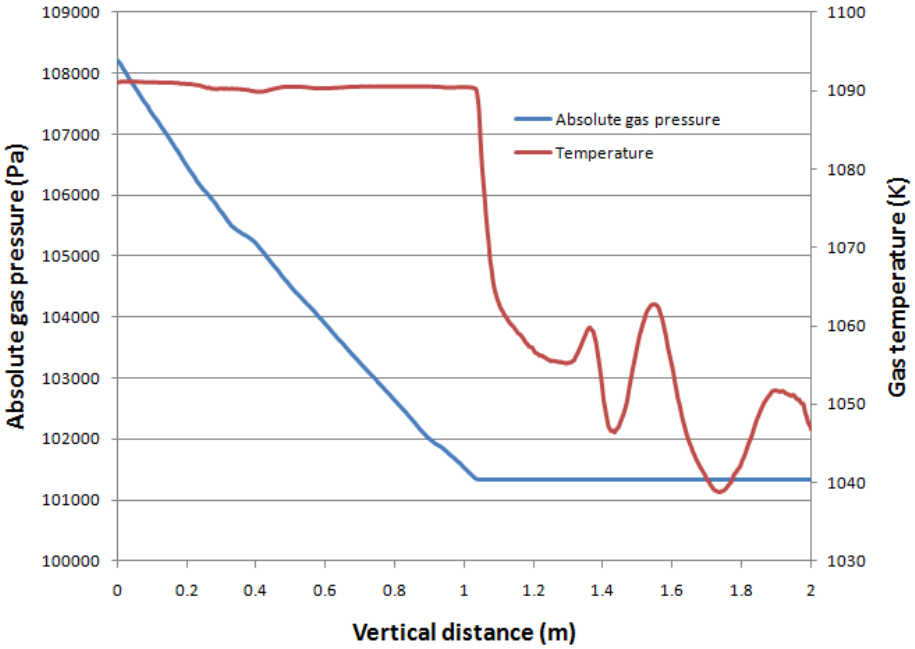

Figure 7.10: Operating conditions of gasifier at t=46 s

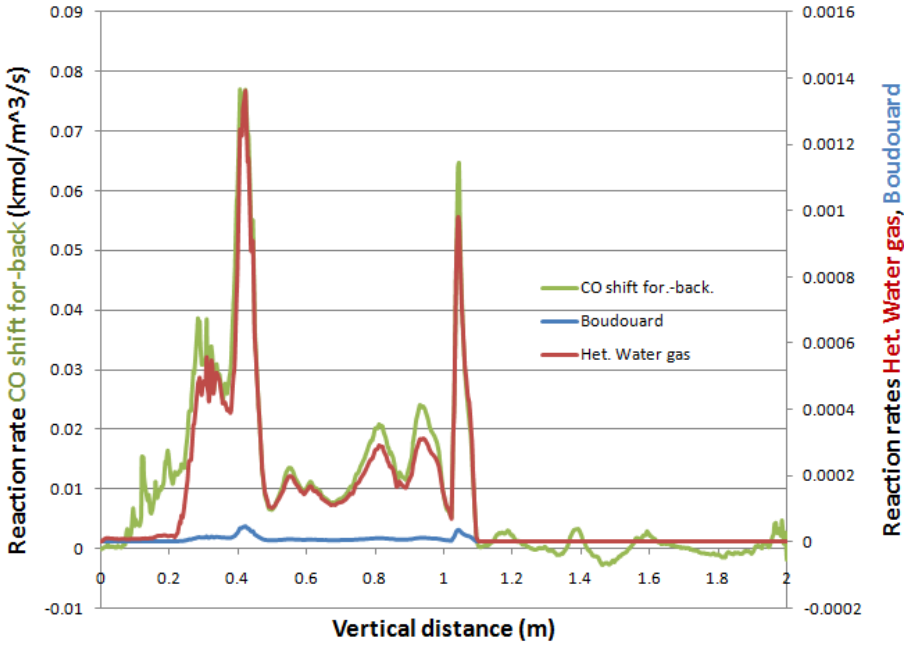

Figure 7.11: Reactions rates at t=46 s

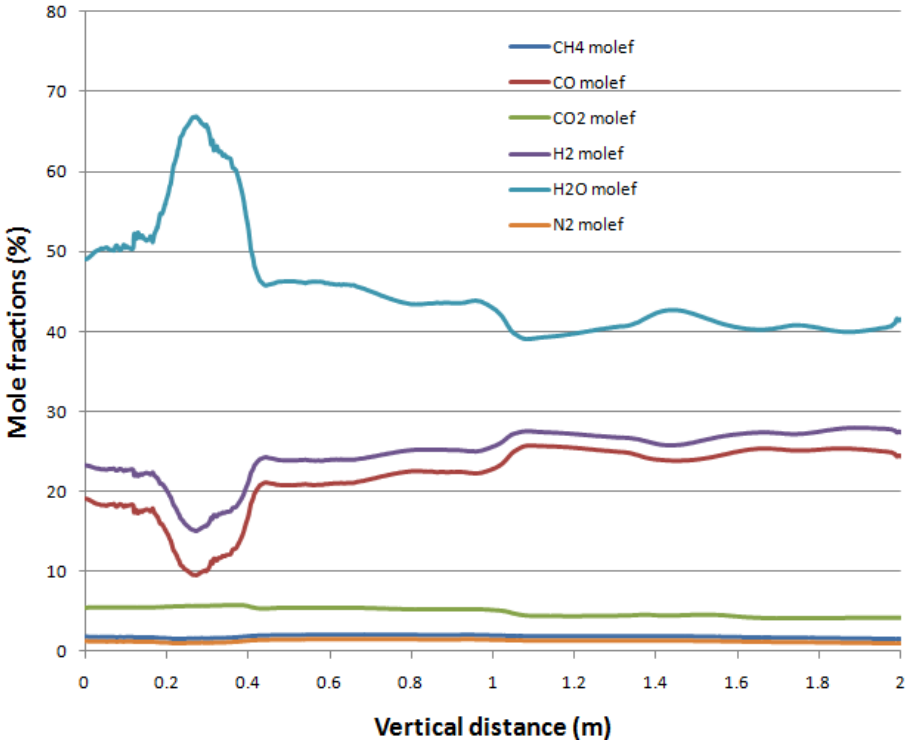

Figure 7.12: Mole fractions at t=46 s

to be calculated through the ultimate analysis, by controlling energy and mass conservation.

2. The reactions rates were taken from literature.

7.3 Revised modelling approach (3^{rd})

After testing the aforementioned approaches, the need for a revised modelling approach emerged. It is obvious that a targeted pyrolysis model had to be developed, in order to better predict the experimental results. The methane pyrolysis model was the first introductory try. The Seebauer model followed, with a more detailed pyrolysis step, concerning wood chips. The present revised model takes into account the proximate and ultimate analysis of the Agrol wood-pellets, in order to calculate the specific composition of the volatile matter.

Given the fuel's proximate and ultimate analysis at Table 6.1, we can calculate the composition of the volatile matter. The procedure is discussed below.

From the proximate analysis we can determine the moles of fixed carbon, which is supposed to be carbon, and the moles of moisture, which is condensed water. From the ultimate analysis we determine the moles of the individual species. To do this, we divide the % weight, by the corresponding molecular weight. The results are shown in Table 7.2.

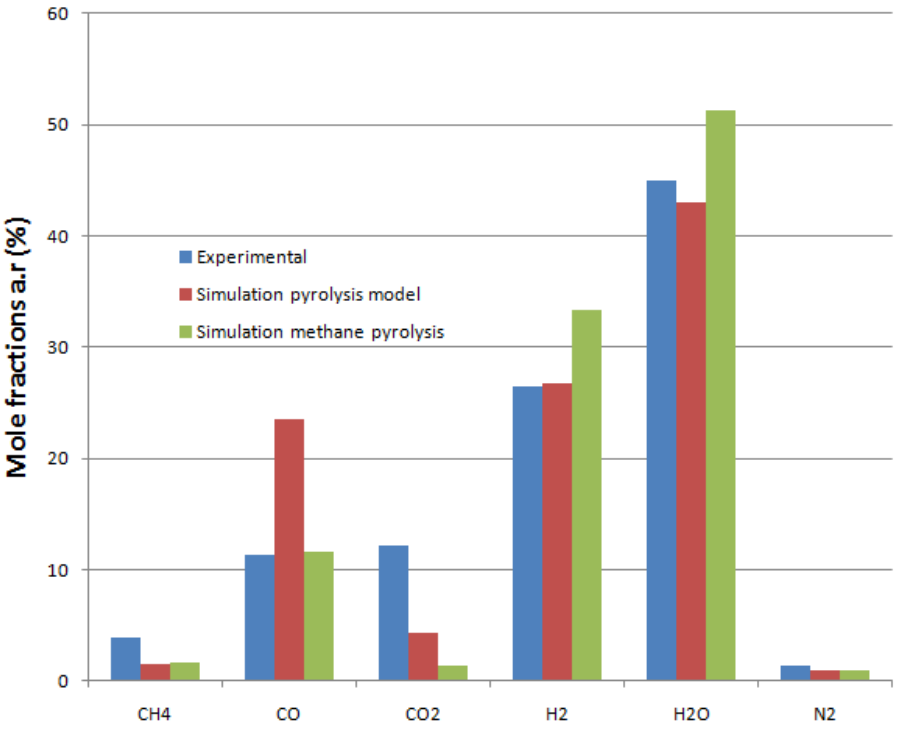

Figure 7.13: Outlet results

Table 7.2: Biomass fuel analysis

Proximate analysis		Molecular mass (kg/kmol)	Moles (kmol/kg fuel)	**Ultimate analysis**		Molecular mass (kg/kmol)	Moles (kmol/kg fuel)
Volatiles (%w/w dry)	81.5	-	-	C	47.4	12.01	0.03946711
Fixed carbon (%w/w dry)	13.6	12.01	0.0113239	H	6.4	1.001	0.06349206
Moisture (%w/w)	4.8	18.016	0.0026643	O	46.0	16.00	0.02875
Ash (Potassium)	0.1	138.205	-	N	0.1	14.008	7.1388E-05
Heating Value				S	0.1	32.066	3.1186E-05
LHV (kJ/kg wet)	20600						

By subtracting the moles engaged in Fixed carbon and moisture from the overall, we can calculate the mole and mass fractions of the species contained in volatiles (Table 7.3).

Table 7.3: Volatile analysis

Volatile species	Moles (kmol/kg fuel)	Mass (kg/kg fuel)
C	0.028143214	0.338
H	0.058163467	0.05862877
O	0.026085702	0.41737123
N	7.13878E-05	0.001
S	3.11857E-05	0.001

As discussed in the current thesis, the volatile matter pyrolyses, through primary and secondary pyrolysis step, giving the gaseous species H_2, CO, CO_2, CH_4, H_2O, and N_2. The amount of these species has to balance the mass and energy (in terms of heating value), of the volatile matter.

The mass balance (Table 7.4) is an iterative process. We assume the pyrolysis species mass fractions, until the volatile mass fractions agree with the given values of Table 7.3. As far as sulphur oxides are not modelled, the S mass fraction will remain zero. This has no significant influence in our case, because S has a very low value.

Table 7.4: Mass balance

Pyrolysis species	Mass fraction (kg/kg fuel)	**Volatile species**	Mass fraction (kg/kg fuel)
H_2	0.01373173	C	0.337970459
CO	0.239092353	H	0.058617908
CO_2	0.379551859	O	0.417411636
CH_4	0.17615033	N	0.001
H_2O	0.00547373	S	0
N_2	0.0001		
SUM	0.815		0.815

Similarly the energy balance is shown in Table 7.5. The energy difference between the pyrolysis and the volatile species is the heat of formation, and subsequently the pyrolysis heat.

Unfortunately, the results from the revised modelling approach are yet to be published. They are expected to better predict the experimental values, and will be published at the author's next work.

Table 7.5: Energy balance

Pyrolysis species	HHV (kJ/kg)	Energy (kJ/kg fuel)	**Volatile species**	HHV (kJ/kg)	Energy (kJ/kg fuel)
H_2	141790	1947.022038	C	34080	11518.03324
CO	10095	2413.637307	H	141790	4155.716619
CO_2	0	0	O	0	0
CH_4	55530	9781.627843	N	0	0
H_2O	0	0	S	9200	0
N_2	0	0			
SUM	-	14142.28719	-	-	15673.74986

7.4 Conclusions

In this work, the related literature was thoroughly investigated. The simulation models achieved in predicting the fluidization character of the fluidized bed reactor, its temperature and pressure distribution. The results from the two (2) approaches are collected in Table 7.6.

Table 7.6: Conclusions

Outlet species	**Methane pyrolysis model**	**Seebauer model**
H_2O	Over-predicted	Fitted
H_2	Over-predicted	Fitted
CO_2	>Under-predicted	Under-predicted
CO	Fitted	Over-predicted

Chapter 8

Prospects

This work aimed in modelling a bubbling fluidized bed reactor, and succeeded in many aspects. Nevertheless, it is not presented as a nostrum, and the future work has to proceed with the following investigation :

- The kinetic parameters of the reactions and validation with experiments
- Specialized pyrolysis model and tar formation through User defined functions (UDF)
- Grid independence control
- Lagrange approach - comparison with Euler approach
- Simulation of various bio-fuels, in order to build a comprehensive predicting tool

Bibliography

[Bioenergy-routes] : *AEBIOM European Biomass Association , Biomass to bioenergy convertion.* – URL `http://www.aebiom.org/?cat=4`

[Fluent] *ANSYS Fluent 13.0 User's Guide*

[Woodpellets] : *Description from Wood-Pellets.* – URL `http://www.woodpellets.com/`

[Oil-Price] : *Price of Petroleum - Wikipedia.* – URL `http://en.wikipedia.org/wiki/Price_of_petroleum`

[Biomass-Potential] : *Survey from the Center of Renewable Sources and Energy Saving about the biomass potential in energy prodution, Greece.* – URL `http://www.cres.gr/energy-saving/images/pdf/biomass_guide.pdf`

[A. Gómez-Barea 2010] A. Gómez-Barea, B. L. ; F., Winter (Hrsg.): *Gasification of Biomass and Waste. Handbook of Combustion.* Wiley-VCH, 2010

[A. Z' Graggen 2008] A. Z' Graggen, A. S.: A two-phase reactor for steam gasification of carbonaceous materials under concentrated trermal radiation. In: *Chemical Engineering and Processing* 47 (2008), S. 655–662

[Alvaro Sanz 2005] Alvaro Sanz, Jose C.: Modeling circulating fluidized bed biomass gasifiers. Results from a pseudo-rigorous 1-dimensional model for stationary state. In: *Fuel Process Technology* 86 (2005), S. 247–258

[B. E. Launder 1974] B. E. Launder, D. B. S.: The Numerical Computation of Turbulent Flow. In: *Computer Methods in Applied Mechanics and Engineering* 3 (1974), S. 269–289

[Blasi 2008] Blasi, Colomba D.: Modeling chemical and physical processes of wood and biomass gasification. In: *Science Direct* 34 (2008), S. 47–90

[Bowen 1967] Bowen, R. M. ; Eringen, A. C. (Hrsg.): *Theory of mixtures. In Continuum Physics.* New York: Academic Press, 1967

[C. A. Koufopanos 1989] C. A. Koufopanos, A. L.: Kinetic modeling of the Pyrolysis of Biomass and Biomass Components. In: *The Canadian Journal of Chemical Engineering* 67 (1989), S. 75–83

[C. Franco 2002] C. Franco, I. Gulyurtlu I. C.: The study of reactions influencing the biomass steam gasification process. In: *Fuel* 82 (2002), S. 835–842

[C. K. K. Lun 1984] C. K. K. Lun, D. J. Jeffrey N. C.: Kinetic Theories for Granular Flow: Inelastic Particles in Couette Flow and Slightly Inelastic Particles in a General Flow Field. In: *The Journal of Fluid Mechanics* 140 (1984), S. 223–256

[C. Lucas 2004] C. Lucas, W. Blasiak S. M.: High temperature air and steam gasification of densified biofuels. In: *Biomass and Bioenergy* 27 (2004), S. 563–575

[C. Mandl June/July 2009] C. Mandl, F. B.: Updraft fixed-bed gasification of softwood pellets : Mathematical modeling and comparison with experimental data. In: *17th European biomass conference and exhibition, Hamburg, ETA-Renewable Energies (Ed.), Italy*, June/July 2009

[C.-Y. Wen 1966] C.-Y. Wen, Y. H. Y.: Mechanics of Fluidization. In: *Chemical Engineering Progress Symposium Series* 62 (1966), S. 100–111

[Christopher Higman 2008] Christopher Higman, Maarten J. van der B. ; Elsevier (Hrsg.): *Gasification*. Gulf Professional Publishing, 2008

[D. Gidaspow 1992] D. Gidaspow, J. D.: Hydrodynamics of Circulating Fluidized Beds, Kinetic Theory Approach. In: *Fluidization VII, Proceedings of the 7th Engineering Foundation Conference on Fluidization, 75-82*, 1992

[D. Lathouwers 2001a] D. Lathouwers, J. B.: Modelling of dense gas-solid reactive mixtures applied to biomass pyrolysis in a fluidized bed. In: *International Journal of Multiphase Flow* 27 (2001), S. 2155–2187

[D. Lathouwers 2001b] D. Lathouwers, J. B.: Yield optimization and scaling of fluidized beds for tar production from biomass. In: *Energy Fuels* 15 (2001), S. 1247–1262

[D. Ma 1990] D. Ma, G. A.: A Thermodynamical Formulation for Dispersed Multiphase Turbulent Flows. In: *International Journal of Multiphase Flow* 16 (1990), S. 323–351

[D. Sofialidis 2001] D. Sofialidis, O. F.: Simulation of biomass gasification in fluidized beds using computational fluid dynamics approach. In: *Thermal Science* 5(2) (2001), S. 95–105

[E.D. Gordillo 2011] E.D. Gordillo, A. B.: A two phase model of high temperature steam-only gasification of biomass char in bubbling fluidised bed reactors using nuclear heat. In: *International Journal of Hydrogen Energy* 36 (2011), S. 374–381

[Ergun 1952] Ergun, S.: Fluid Flow through Packed Columns. In: *Chemical Engineering Progress Symposium Series* 48(2) (1952), S. 89–94

[FAO] FAO: *Food and Agriculture Organization of the United Nations (FAO), Types of gasifiers.* – URL `http://www.fao.org/docrep/t0512e/T0512e0a.htm`

[Fennell PS 2005] Fennell PS, Dennis J.: The kinetics of oxidation of chars from three different coals, as measured in fluidized beds. In: *18th International Conference on Fluidized Bed Combustion*, 2005, S. 881–894

[G. Schuster 2001] G. Schuster, K. Weigl H. H.: Biomass steam gasification – an extensive parametric modeling study. In: *Bioresource Technology* 77 (2001), S. 71–79

[Gronli 1996] Gronli, M. G.: *A theoretical and experimental study of the thermal degradation of biomass*, NTNU, Trondheim, Norway, Dissertation, 1996

[J. Ding 1990] J. Ding, D. G.: A Bubbling Fluidization Model Using Kinetic Theory of Granular Flow. In: *AIChE* 36(4) (1990), S. 523–538

[J. Larfeldt 2000] J. Larfeldt, M.C. M.: Modelling and measurements of the pyrolysis of large wood particles. In: *Fuel* 79 (2000), S. 1637–1643

[J. Rath 2001] J. Rath, S. S.: Craking Reactions of Tar from Pyrolysis of Spruce Wood. In: *Fuel* 80 (2001), S. 1379–1389

[J.C. Wurzenberger 2002] J.C. Wurzenberger, H. Raupenstrauch J.G. K.: Thermal conversion of biomass: Comprehensive reactor and particle modeling. In: *AIChE Journal* 48 (2002), S. 2398–2411

[K. Papadikis 2008] K. Papadikis, S. G.: CFD modelling of the fast pyrolysis of biomass in fluidised bed reactors, Part A: Eulerian computation of momentum transport in bubbling fluidised beds. In: *Chemical Engineering Science* 63 (2008), S. 4218–4227

[Liang Yu 2007] Liang Yu, Xiangping Zhang Suojiang Z.: Numerical simulation of the bubbling fluidized bed coal gasification by the kinetic theory of granular flow (KTGF). In: *Fuel* 86 (2007), S. 722–734

[M. Syamlal 1993] M. Syamlal, T. J. O.: MFIX Documentation: Volume1, Theory Guide / National Technical Information Service, Springfield, VA. DOE/METC-94/1004, NTIS/DE94000087. 1993. – Forschungsbericht

[Michael Oevermann 2009] Michael Oevermann, Frank B.: Euler-Lagrange/DEM simulation of wood gasification in a bubbling fluidized bed reactor. In: *Particuology* 7 (2009), S. 307–316

[M.J. Boroson 1989] M.J. Boroson, J. H.: Product yields and kinetics from vapor phase cracking of wood pyrolysis. In: *AIChE Journal* 35 (1989), S. 120

[Prabir Basu 2009] Prabir Basu, Kaushal P.: Modeling of Pyrolysis and Gasification of Biomass in Fluidized Beds: A Review. In: *Chemical Product and Process Modeling* 4 (2009), S. Iss. 1, Article 21

[Priyanka Kaushal 2010] Priyanka Kaushal, Nader M.: A comprehensive mathematical model for biomass gasification in a bubbling fluidized bed reactor,. In: *Fuel* 89 (2010), S. 3650–3661

[R. Reimert 1989] R. Reimert, G. S.: Gas Production. In: *Ullman's Encyclopedia of Industrial Chemistry* 5th edn, Vol A 12. Weinheim: VCH Verlagsgesellschaft (1989), S. pp.215

[S. Gerber 2010] S. Gerber, M. O.: An Eulerian modeling approach of wood gasification in a bubbling fluidized bed reactor using char as bed material. In: *Fuel* 89 (2010), S. 2903–2917

[S. Karellas 2008] S. Karellas, T. Papadopoulos C. Schäfer J. K.: Hydrogen production from allothermal biomass gasification by means of palladium membranes. In: *Fuel Processing Technology* 89 (2008), S. 582–588

[Schaeffer 1987] Schaeffer, D. G.: Instability in the Evolution Equations Describing Incompressible Granular Flow. In: *Journal of Differential Equations* 66 (1987), S. 19–50

[Seebauer 1999] Seebauer, V.: *Experimentelle Untersuchungen zur Pyrolyse von Kohle und Holz*, Graz University of Technology, Dissertation, 1999

[Smoot L.Douglas 1985] Smoot L.Douglas, Smith Philip J.: *Coal combustion and gasification.* Plenum Press, 1985

[S.T. Sie 1999] S.T. Sie, R. K.: *Applied Catalysis A: General 186, 55-70.* 1999

[Syamlal 1987] Syamlal, M.: The Particle-Particle Drag Term in a Multiparticle Model of Fluidization / National Technical Information Service, Springfield, VA. 1987. – Forschungsbericht

[T. B. Anderson 1967] T. B. Anderson, R. J.: A Fluid Mechanical Description of Fluidized Beds. In: *I and EC Fundamentals* 6 (1967), S. 527–534

[Wikipedia] Wikipedia: *Article of Wikipedia on biomass gasification.* – URL `http://en.wikipedia.org/wiki/Biomass_gasification`

[Y. Wang 1993] Y. Wang, C.M. K.: Kinetic model of biomass gasification. In: *Solar Energy* 51 (1993), S. 19–25